Urban Climate 42 (2022) 101109

Contents lists available at ScienceDirect

Urban Climate

journal homepage: www.elsevier.com/locate/uclim

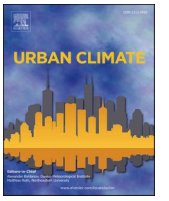

Observed sea breeze life cycle in and around NYC: Impacts on UHI and ozone patterns

Z.S. Han [a,b,*], J.E. González-Cruz [b,d], H.N. Liu [a], D. Melecio-Vázquez [b,d], H. Gamarro [b,d], Y.H. Wu [c,d], F. Moshary [c,d], R. Bornstein [e]

[a] School of Atmospheric Sciences, Nanjing University, Nanjing, Jiangsu, China
[b] Department of Mechanical Engineering Department, The City College of New York, New York, NY, USA
[c] Optical Remote Sensing Laboratory, The City College of New York, NY, USA
[d] NOAA Cooperative Science Center for Earth System Science and Remote Sensing Technologies, The City College of New York, New York, NY, USA
[e] Department of Meteorology and Climate Science, San Jose State University, San Jose, CA, USA

ARTICLE INFO

Keywords:
Ozone episodes
Urban heat islands
Sea breeze fronts
Regional heat waves

ABSTRACT

This observational study investigates New York City (NYC) impacts on summer sea breeze fronts (SBFs) during a 2018 LISTOS Campaign day with a regional heat wave and O_3 episode. A morning urban heat island peaked at 8.3 °C and then induced convergences into the City, trapping its NO_2 emissions. SBFs came ashore at 0700 EST from the Atlantic along southern Long Island (LI), and from the LI Sound along northern LI and southern Connecticut; 2-h later another formed over New Jersey. The Ocean front was retarded over NYC at noon, while all fronts merged by 1400 EST and continued inland for four more hours. High O_3 first appeared at 0900 EST downwind of NYC. By 1100 EST, a new surface peak formed north of the City in the Hudson River Valley (HRV). The maxima merged, peaking at 143 ppb at 1300 EST behind the SBF and near the maximum temperatures of 39 °C. Trajectories ending at the northern LI site with a PBL O_3 peak first passed NYC, arrived before the episode, and then recirculated back in its SB flow. Trajectories ending in the HRV showed pollutant transport over NYC twice, before advection northward into the narrow Valley by the ocean SBF.

1. Introduction

More than half the global population lives in urban areas, increasingly in high-density coastal cities (Ritchie and Roser, 2018; UN, 2018). Urbanization creates new local climates via changes to regional surface and atmospheric properties, often associated with increased energy demand, air pollutants, and heat emissions (Bornstein, 1968; Ongoma et al., 2013; Melecio-Vázquez et al., 2018). These processes lead to altered microclimates, including urban heat islands (UHIs), defined as the excess warmth of a city over its surrounding rural areas (Grimmond, 2007; Stewart and Oke, 2012). Strong UHIs produce convergent winds into their centers, while with weak UHIs, regional speeds are reduced over these centers (Bornstein and Johnson, 1977). Cities are thus vulnerable to heat wave conditions (Tan et al., 2010; Li and Bou-Zeid, 2013; Ortiz et al., 2019) and the leading cause of US weather-related fatalities is heat stress (NWS, 2015). Most megacities (70%) are in less-developed global regions, and 78% are coastal (Pullen et al., 2007). Coastal cities experience sea breezes, which provide cooling (Yamamoto and Ishikawa, 2020) and affect air quality (Seaman and Michelson,

* Corresponding author at: School of Atmospheric Sciences, Nanjing University, Nanjing, Jiangsu, China.
E-mail address: mg1628027@smail.nju.edu.cn (Z.S. Han).

https://doi.org/10.1016/j.uclim.2022.101109
Received 13 July 2021; Received in revised form 21 January 2022; Accepted 21 January 2022
Available online 3 February 2022

2000). Such breezes arise from the contrasting thermal responses of land and water surfaces, i.e., a near-surface onshore atmospheric pressure gradient forms, from the cool sea to the hot land (Simpson, 1994).

A variety of sea breezes types can arise (Tijm and van Delden, 1999). In otherwise calm circumstances, a closed circulation cell develops at the coast (Holton, 1992), which grows horizontally and vertically. With a weak opposing offshore regional flow, an inland moving sea breeze front (SBF) develops in the near calm convergence zone between the two flows (Hsu, 1988). A convective internal boundary layer with a capping inversion thus forms within the landward moving marine air mass (Zhong and Takle, 1992). Surface frictional retardation creates an upper-level frontal "nose," which passes earlier than the surface front. The SB head may be as deep as 700 m, but the elevated inversion transition-layer is only several tens of meters thick. SBFs are thus also associated with complex vertical motions, with the primary updraft in the convergence just ahead of the SBF as the denser marine air undercuts the lighter continental air (Simpson, 1997). Cumulus cloud lines associated with these upward motions have been observed in satellite images (Ferdiansyah et al., 2020). With an onshore-directed regional flow, however, SBFs are only higher speed pulses onto the existing onshore flow (Rao and Fuelberg, 2000). With reduced late afternoon inland heating, all SBFs retreat to the coast as a land breeze (Simpson et al., 1977).

Urban areas retard SBF inland movement due to surface-roughness/building-barrier effects (Boucouvala and Bornstein, 2003), while UHI convergence enhances SBF convergence zones (Ferdiansyah et al., 2020). The diurnal cycles of surface pollutant concentration are complicated by SBFs, as their convergent surface winds (Loughner et al., 2011) and capping inversions (Darby et al., 2007) produce accumulation. Other impacts include early morning offshore precursor transport (Ding et al., 2004) and reduced dry deposition in their stable marine air (Lenschow et al., 1981). Recirculated polluted air onshore by a next-day SBF (Wentworth et al., 2015) and downward fumigation of elevated-layers (Lyons et al., 1981) can, however, produce local late morning pollutant maxima.

New York City (NYC) metro area SBFs have been previously investigated because of the complex flow patterns from the Atlantic Ocean and Long Island Sound (LIS, all acronyms defined in appendix) and right-angled coastline at the intersection of NYC and New Jersey (NJ, Fig. 1). Frizzola and Fisher (1963) were the first to investigate the SBF over the south shore of suburban Long Island (LI) and

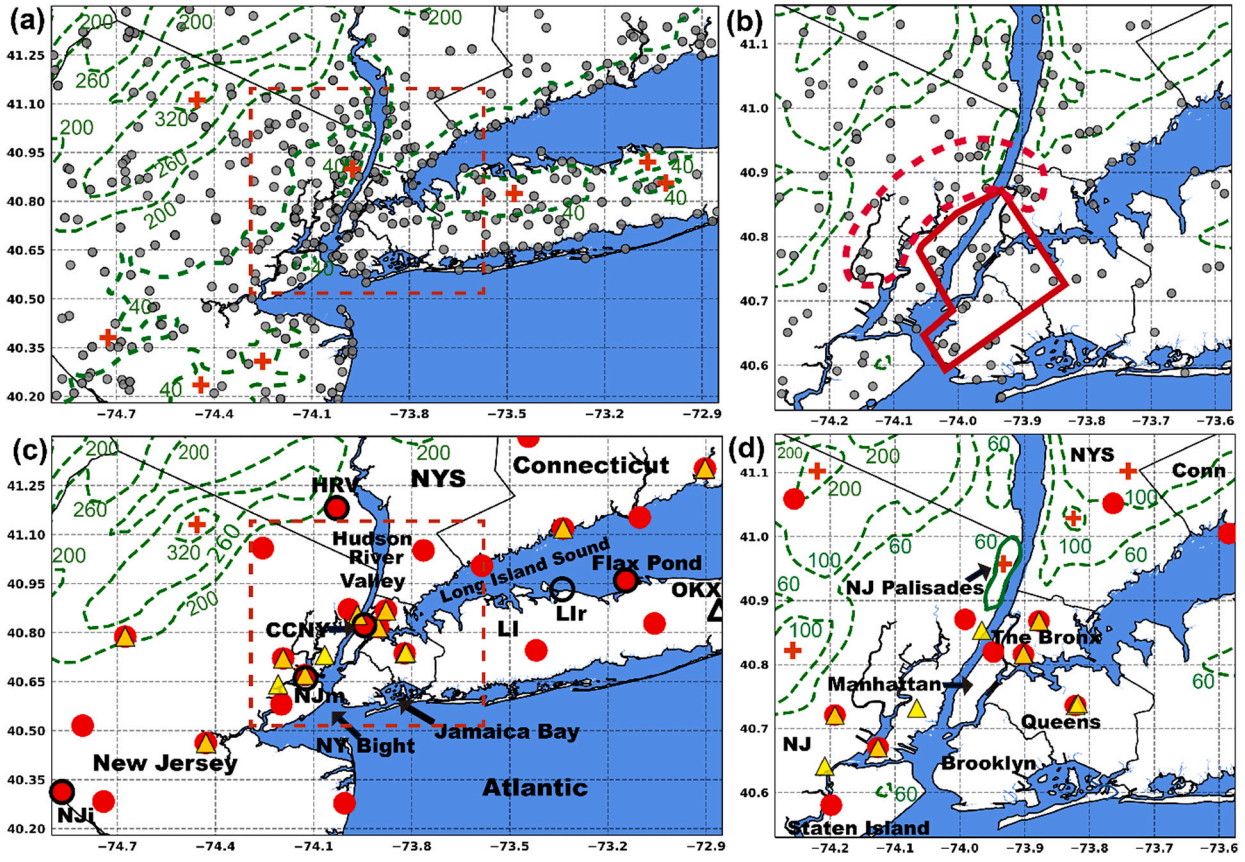

Fig. 1. Meteorological observational sites in (a) outer and (b) inner [also red box in (a)] domains, as well as O_3 (●) and NO_2 (▲) sites in (c) and (d). In (b) The outlines of urban (red solid) and rural (red dashed) areas for UHI calculations are shown in (b), while (c) shows Fig. 5 sites (black circles) and OKX radiosonde site (△). Throughout: county boundaries (thin black lines) and key topographic heights (m, green lines), with peak terrain points (+). US States include NYS, Conn., and NJ, while NYC boroughs are Manhattan, Brooklyn, Queens, Staten Island, and The Bronx; see Appendix for definition of geographic abbreviations. (For interpretation of the references to colour in this figure legend, the reader is referred to the web version of this article.)

the north-south New Jersey (NJ) coast south of NYC. Their data sources included only 11 surface stations, a National Weather Service (NWS) radiosonde, and three pibal balloon sites. On a day with an onshore synoptic flow, the SBF came onshore onto LI at 0900 EST (= GMT- 5 h). It reached its northern shore 4-h later, while in two additional hours its western edge reached Manhattan in NYC. The same synoptic flow on the NJ coast, however, opposed the SB flow, and hence the front only came onshore at 1200 EST. The 1900 EST NWS sounding showed a weak SBF inversion. The remaining two days in the study had strong opposing synoptic flows and thus slowed frontal penetrations. The events showed that as opposing speeds increased, SB flows were shallower, had lower speeds, and reduced inland penetrations.

While the above study could not focus on NYC urban impacts on SBFs due to limited surface sites, Bornstein and Anderson (1980) and Bornstein and Thompson (1981) used a more extensive data network of 97 sites from the NYU/NYC Urban Air Pollution Dynamics Project. Given an opposing synoptic flow in their case study, fronts first came onshore at 1200 EST at the southern LI and NJ coasts. The NYC urban building morphology, however, severally retarded it over Manhattan, distorting its shape; it finally passed the City at 1900 EST. Similar effects on weak cold fronts moving over NYC had been found by Loose and Bornstein (1977).

A climatological study of NYC area SBFs by Gedzelman et al. (2003) showed daytime UHIs both delayed in formation and reduced in frequency during SBF periods. During a regional heat wave, strong westerly winds suppressed the SBF, and thus the City recorded its all-time high March temperature. Novak and Colle (2006) used surface data from 220 surface stations to study the evolution of SBFs across the NYC area on a single day. Three fronts formed by 0900 EST on the: southern and northern LI coasts and southern Connecticut coast. Two hours later, the Connecticut front had not moved, the weak northern LI front was no longer discernable, and the third had moved northward to central LI. Four hours later, the remaining two fronts merged and passed NYC.

The Frizzola and Fisher (1963) study (discussed above) also calculated SBF vertical slopes by use of surface and PBL observations. Slopes outside of NYC were generally about 1:100, but at their leading SBF edge, they steepened to 1:20. Bornstein (1987a, 1987b) evaluated SBF slopes via the NYU/NYC surface winds (discussed above), along with 3-D tetroon positions and helicopter soundings. Slopes steepened over NYC due to building-induced surface retardation of its surface movement, in combination with the lack of retardation aloft, producing slopes up 1:2 over the City. Large and deep vertical velocities during the daytime convective conditions were also observed. Similar frontal steeping was also seen during weak cold front passages over NYC by Gaffen and Bornstein (1988).

SBF effects on SO_2 concentrations were first investigated by Bornstein and Thompson (1981) during the SBF event discussed above by use of data from 33 surface sites. Results showed early morning offshore transport of polluted air by the synoptic flow, followed by reduced concentrations at coastal sites at 1200 EST as clean air was advected onshore behind the SBF. Values behind the inland moving front, however, increased due to fresh emissions into the marine air. Gaza (1998) evaluated SBF impacts on NYC area O_3 concentrations. They used surface and upper air data, as well as O_3 concentrations at 22 surface sites. By 1400 EST, an SBF along the south shore of Connecticut was 30 km north of NYC and was associated with an east to west O_3 peak behind the front. The peak was not a continuous plume from NYC, but a northward-moving band aligned with the east-west oriented front. Zhang et al. (1998) also used data from instrumented aircraft to study that same day. They showed O_3 build-up in a nocturnal elevated residual layer, while subsequent fumigation to the ground rapidly (but only temporarily) increased morning NYC concentrations. The timing of an O_3 peak along the Connecticut River north of NYC suggested transport by the SBF in combination with valley channeling.

Aircrafts were also used by Lee et al. (2011) to study the transport and transformation of NYC area O_3. When synoptic winds changed to offshore/westerly around 1130 EST, both aircraft captured strong offshore City plumes at downwind ocean sites. The plumes had extended upwards to 2 km near NYC but shrank to 1 km over the stable marine boundary layer (MBL), which was vertically decoupled from the ocean surface. Mobile measurements, lidar wind profiles, NO_2 column concentrations, and satellites were used by Zhang et al. (2020, 2021) to study SBF influences on LI surface O_3 and $PM_{2.5}$ distributions during the 2018 Long Island Sound Tropospheric Ozone Study (LISTOS). Results showed that the front developed on its southern shore at 1100 EST, and when it passed the northern shore 5-h later it brought high concentrations. Back trajectories from the Hybrid Single-Particle Lagrangian Integrated Trajectory (HYSPLIT) model ending at the southern shore showed that NYC emissions were first transported out over the ocean and then were contained within the shallow MBL, where photochemical O_3 production occurred. The O_3 was finally transported back inland near the surface by the SBF.

Whereas previous studies of NYC metropolitan area O_3 episodes have focused on some aspects of the many complex interactions between the synoptic conditions, coastal shape, PBL processes, and UHI and building-barrier impacts, the current effort more fully investigates the interactions between all these factors. The study focuses on a five-day summer period with a synoptic-scale heat wave and associated regional O_3 episode during a data-rich 2018 LISTOS Intensive Observational Period (IOP) campaign.

2. Methodology

The regional O_3 episode that impacted the NYC area on 2 July 2018 occurred during a four-day regional heat wave that started on 30 June and was associated with a complex local sea-land breeze system. Hourly surface O_3 concentrations of >140 ppb were twice the US Environmental Protection Agency (EPA) National Ambient Air Quality Standard (NAAQS) of 70 ppb, herein "the standard," but ignoring the 8-h running-average aspect. PBL data used in the study are from LISTOS (http://www.nescaum.org/documents/listos), whose data are stored at: https://www-air.larc.nasa.gov/missions/listos/index.html.

Scientific questions addressed herein include how the extensive surface and PBL observations from a LISTOS IOP can provide a better understanding of how: (a) NYC UHIs and building barriers impact the movement of the: photochemical precursor emissions, multiple SBFs that form along the complex coastlines, and O_3 peaks at the surface and within the PBL; (b) regional heat waves exacerbate area O_3 peaks, and (c) all the above interact to produce concurrent surface O_3 maxima within and downwind of NYC.

2.1. Data

Two observational domains were used, i.e., an outer one (Fig. 1a) that encompasses NYC and its surrounding areas and a zoomed-in sub-domain over the City (Fig. 1b). The 30-arc-second (1 km) terrain data from the US Geological Survey's 2010 Global Multi-resolution Terrain Elevation dataset (U.S. Geological Survey, 2010; https://www.usgs.gov/centers/eros/science/) resolved key area features. The highest peak (424 m) is in the northwest corner of the outer domain (Fig. 1a), with only its surroundings elevations >200 m, with less significant terrain (>40 m) over the Connecticut and NJ coasts and the north shore of LI. Within the smaller domain (Fig. 1d), the most significant terrains (>60 m) are in the: NJ Palisades across the Hudson River from Manhattan, NJ hills at western edge of the domain, NYS area north of NYC, and north shore of LI.

Hourly 2-m temperature and 10-m wind velocities were obtained from 364 stations (Fig. 1a) within 11 networks (Table 1); these levels are hereafter referred to as the "surface." They were downloaded from the City College of New York (CCNY) NOAA-Center for Earth System Sciences and Remote Sensing Technologies (CESSRST), part of its NYCMetNet in its Optical Remote Sensing Lab (https://datadb.noaacrest.org/public/ORSL/Archived_MADIS/). Of these, 119 sites (Fig. 1b) from eight networks are mostly within the NYC sub-domain (Table 1). Values within 5 min of the hour were assumed at the hour. The temperature (T) and velocity (V) networks are reasonably dense in NYC, except in the area north of Jamaica Bay (Fig. 1b).

Data from NWS sites are provided to the Meteorological Assimilation Data Ingest System (MADIS) as whole-value knots, while those from other sources are converted to closest whole-value knots. When downloaded from MADIS in units of m/s, they are reconverted back to m/s and thus can only have a finite number of values, each corresponding to a whole knot value converted to m/s, e.g., 1 kt = 0.44 m/s and 2 kt = 0.88 m/s (Automated Surface Observing System (ASOS) User's Guide, National Oceanic, and Atmospheric Administration, Department of Defense, Federal Aviation Administration, United States Navy, 1998https://www.weather.gov/media/asos/aum-toc.pdf). The current effort ignores all MADIS values <0.5 m/s and thus eliminates all original observations of 1 kt and 1 mph. This cutoff was selected as such low-speed directions are unreliable. MADIS data have passed a three-step QA/QC procedure: level-1 for validity; level-2 for internal, temporal, and statistical consistencies; and level-3 for spatial consistency. The UrbaNet data needed to be QA/QC-ed in-house with this procedure, documented in NWS Techniques Specification Package 88–21-R2 (Technique Specification Package, 1994, https://www.wpc.ncep.noaa.gov/archives/).

Hourly surface O_3 and NO_2 concentrations were provided by the US EPA Air Quality System (EPA-AQS, https://aqs.epa.gov/aqsweb/airdata/download_files.html) at 25 and 13 sites in the outer domain, respectively (Fig. 1c and Table 1), with 11 and nine of these, respectively, in the inner domain (Fig. 1d). These measurements were also fully QA/QC-ed, with EPA procedures described at https://www.epa.gov/aqs. Daily O_3 Air Quality Index (AQI) maps were downloaded from the EPA AirNow website (https://www.airnow.gov) for 1 and 2 July. If a site records an 8-h peak-average O_3 value of 70 ppb (the EPA criteria level) anytime during a 24-h period, then the site has a daily AQI value of 100. The scale is linear, so peak averages of 140 ppb produce an AQI of 200. These values are related to human health impacts in Table 2. Meta-data for all meteorological and air quality sites are at the websites cited above. The Natural Neighbor Interpolation (NNI) scheme of Sibson (1981) was used on the surface T, O_3, and NO_2 data. It uses 2-D triangulation to connect all pairs of neighboring data points; details can be found in Okabe et al. (2000). Areas with the fewest sites in the O_3 network are on the plain southeast of the NJ hills and in the NO_2 network are north of NYC (Fig. 1c). So isolines are more approximate in those areas.

Upper-air meteorological data were obtained at 0700 and 1900 EST on 1 and 2 July from the NWS radiosonde station OKX at Upton, LI, 100 km east of NYC (Fig. 1c). The balloon ascent rate is about 5 m/s, and T, potential temperature (θ), and relative humidity (RH) values within the lowest 2 km (AGL, used hereafter unless otherwise stated) were downloaded from the Wyoming Weather Web page (http://weather.uwyo.edu/upperair/sounding.html). Because large variations exist within a RH sounding, values were smoothed via a five-point centered running average, with the first point kept as reported and a three-point average used for the second point. No averaging was necessary for the T and θ values.

Table 1
Number of meteorological, O_3, and NO_2 sites in each network within the study area ('Total'), plus of those, the number in the ('Inner') NYC sub-domain.

Networks	Inner	Total
*AWS (Automatic Weather Station Tower, Earth Networks)	30	100
*NJWxNet (New Jersey Weather and Climate Network)	5	19
*NYSM (NYS Mesonet)	6	8
*WxFlow (WeatherFlow, Inc.)	5	17
*UrbaNet (EarthNetworks, Inc)	20	20
APRSWXNET (Citizen Weather Observers Program)	51	182
HADS (Hydrometeorological Automated Data System)	0	2
NONFedAWOS (Non-Federal AWOS)	0	6
NOS-NWLON (Nat. Ocean Service Water Level Obs. Network)	0	2
NOS-PORTS (NOS Physical Oceanographic Real-Time System)	1	2
RAWS (Remote Automated Weather Stations)	1	6
Total meteorological stations	*119*	*364*
AQS O_3 (Air Quality System, EPA)	11	25
AQS NO_2	9	13

Note. *() are National Mesonet providers.

Table 2
US EPA daily ozone air quality index (AQI, no units) classes and O_3 (ppb) values; descriptions are for general populations except where noted.

Description	AQI Values	O_3 (ppb)
Good	0–50	0–35
Moderate	51–100	35–70
Unhealthy for Sensitive Groups	101–150	70–105
Unhealthy	151–200	105–140
Very Unhealthy	201–300	140–210

Five LISTOS balloon sondes recorded vertical profiles of O_3, T, θ, V, and RH during the study period at the Flax Pond Marine Laboratory, on the rural north shore of LI (Fig. 1c). Vaisala radiosondes with an Ensci Electrochemical Cell ozonesonde provided data at 1 Hz intervals, with an uncertainty of 5–10% in the troposphere. Only data within the lowest 2 km were used from launches at 0500 and 1300 EST on 1 July and at 0100, 1200, and 1500 EST on 2 July. First level values in each sounding were not considered as they were: (a) listed as the zero second values at a height of 4.4 m, while those after 1-s were listed at 5.5 m (reasonable given the average rate of rising of about 5 m/s) and (b) inconsistent with those at levels 2 to 4 in the same launch and with those at nearby surface sites. The remaining RH and V (speed and direction) values were smoothed via 5- and 30-point averages, respectively. The new first point was kept as calculated and a three-point average was again used for the new second point.

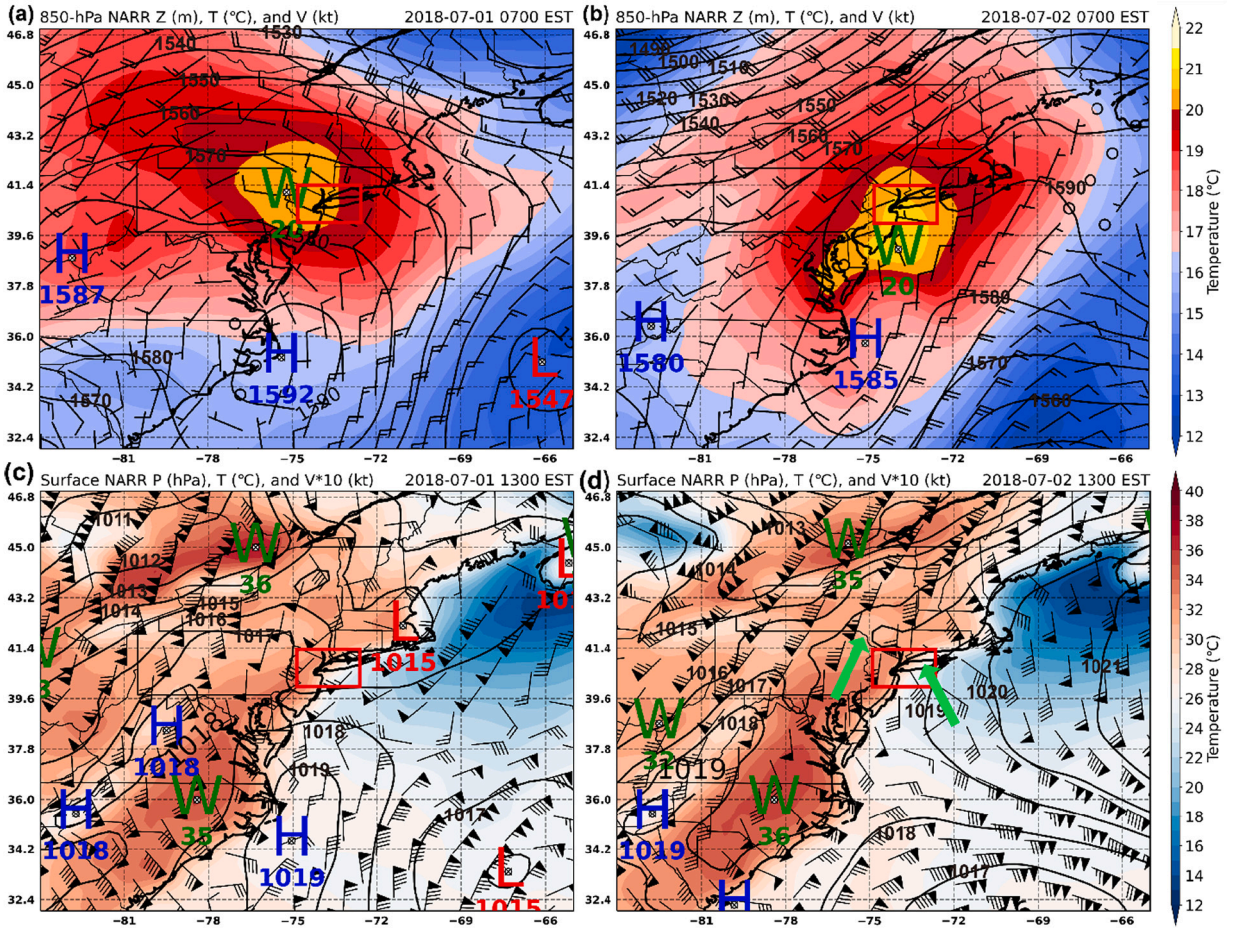

Fig. 2. NARR 850 hPa charts (upper) over the eastern US at 0700 EST on (a) 1 July and (b) 2 July 2018, with geopotential heights (solid lines, interval of 10 m), wind vectors (1 full barb is 10 kts), and isotherms (°C, colors), where the red box is the outer domain of Fig. 1. NARR surface charts (lower row) at 1300 EST on (c) 1 July and (d) 2 July show sea-level isobars (solid lines, interval of 1 hPa), wind vectors (1 full barb is 1 kt and flag is 5 kts), and temperatures (°C, colors). High (H) and low (L) pressure centers and warm areas (W) are shown, along with subjectively placed area-average wind vectors (green arrows) in (d). (For interpretation of the references to colour in this figure legend, the reader is referred to the web version of this article.)

2.2. Analyses

Nocturnal 2-m level UHI values were calculated from 19 NYC sites and from 15 fewer urban (hereafter "rural") sites west of the City (Fig. 1b). The area containing the urban sites best illustrated the horizontal extent of the high NYC temperatures, while the area of the rural sites forms a ring around the City at locations not influenced by either the hills to their west or the water bodies to their east. UHI magnitude was defined as the difference between the warmest of the 19 urban and coolest of the 15 rural sites at each hour.

As the SBF over NYC on 2 July generally involved only a pulse of marine air with an increased speed on top of a regional onshore flow, its inland movement required careful analysis. The following seven factors were thus used to determine its positions: (i) directional convergence, as wind directions shift across an SBF, (ii) post-frontal speed increases in the pulse of the SB air, (iii) pre-frontal calm speeds, as speeds are low within an SB convergence zone, (iv) temperature differences at inland sites, as the current "pulse" type SBF produces only minimal coastal cooling as it passes, (v) coastal shape, including Jamaica Bay and the various inlets of the New York Bight, (vi) spatial and/or hourly consistency, and (vii) details gleaned from zoom-ins over NYC. NYC provided additional

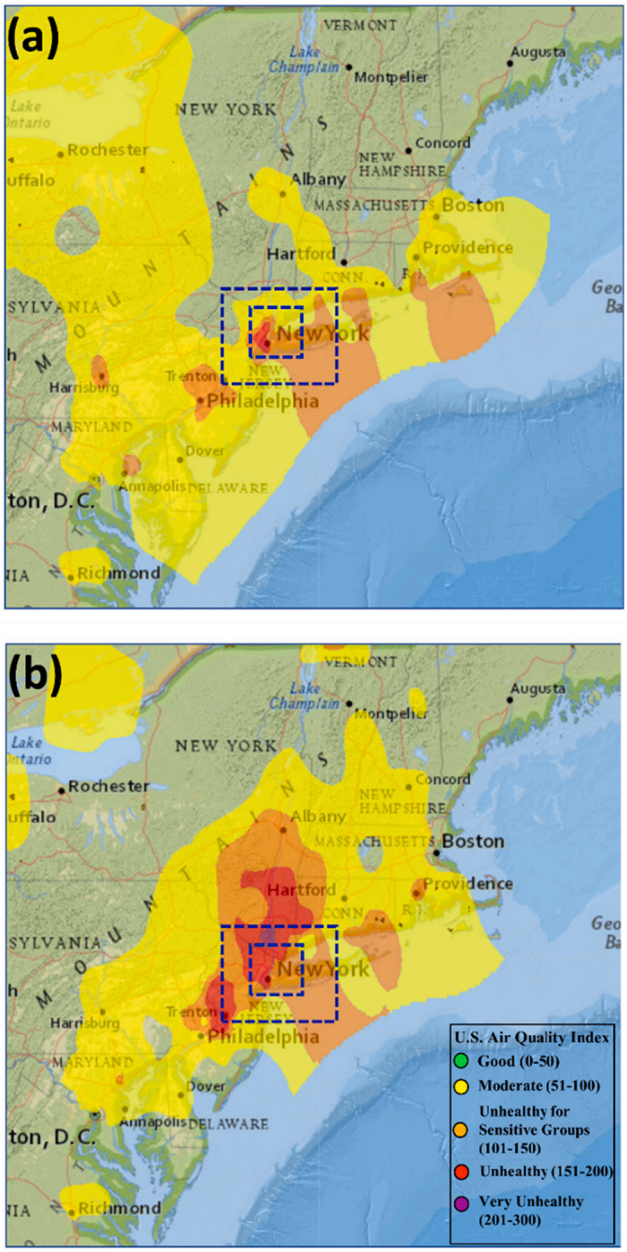

Fig. 3. EPA daily O_3 Air Quality Index Values (AQI, no units) for (a) 1 and (b) 2 July, with EPA Alert-Ranges (insert) and inner and outer domains (dashed boxes) of Fig. 1.

challenges, due to the relative scarcity of sites within a few areas of the City (Fig. 1b) and the somewhat chaotic nature of urban winds. Investigation of the NYC wind network metadata, however, has shown that the instruments are generally well-sited and are capable of yielding coherent wind flow patterns (Bornstein and Johnson, 1977, as well as other such NYC studies). Placement of SBF positions in NYC thus relied on spatial and temporal consistency even more than at sites outside of the City.

The origins of the observed high O_3 layer at Flax Pond and of the surface O_3 peak at Hudson River Valley (HRV) site were investigated with back trajectories from the HYSPLIT model (https://www.ready.noaa.gov/ HYSPLIT.php), developed by the NOAA Air Resources Laboratory (ARL, Draxler and Hess, 1998). Horizontal and vertical velocities from the High-Resolution Rapid Refresh NWP model version 1 (HRRRv1) at 3 km and 6-h resolutions were used to drive HYSPLIT. The 24-h trajectories ended at Flax Pond at either 0100 or 1200 EST on 2 July, with model endpoints set at 100, 500, and 1200 m. The 12-h trajectories in the HRV area ended at 1300 EST on 2 July, with the model endpoint set at 10 m. The MATLAB (R2019b) software was used to process the MADIS meteorological, O_3, and NO_2 data for the NNI interpolation process and to plot the Flax Pond sonde profiles. Python version 3 (Van Rossum and Drake, 2009) was used to create the North American Regional Reanalysis (NARR, Mesinger et al., 2006), spatial isopleth, and vector-wind plots. Paint 3-D was used to draw SBF locations and to modify NWS synoptic charts.

3. Results

3.1. Synoptic and regional factors

NARR 32-km resolution charts show that the episode-period synoptic conditions at 850 hPa at 0700 EST on 1 July (Fig. 2a), the day before the O_3 episode, were dominated by a regional weak high-pressure ridge extending northeastward from NYC. On the episode day (Fig. 2b), the ridge is still northeast of NYC but has strengthened and moved closer to the City. Given that NYC was some distance from the high-pressure center (H) on both days, the associated subsidence inversion (not shown) was relatively weak and at a high elevation over the City. The associated flow on 1 July is northwesterly over NYC and adjacent ocean areas, with a northeasterly flow further out to sea. By the episode morning, the 850 hPa winds over the City have changed to generally southwesterly, with a narrow band of northwesterly flow transitioning to the still northeasterly flow over the more distant ocean areas. Concurrent temperatures on 1 July

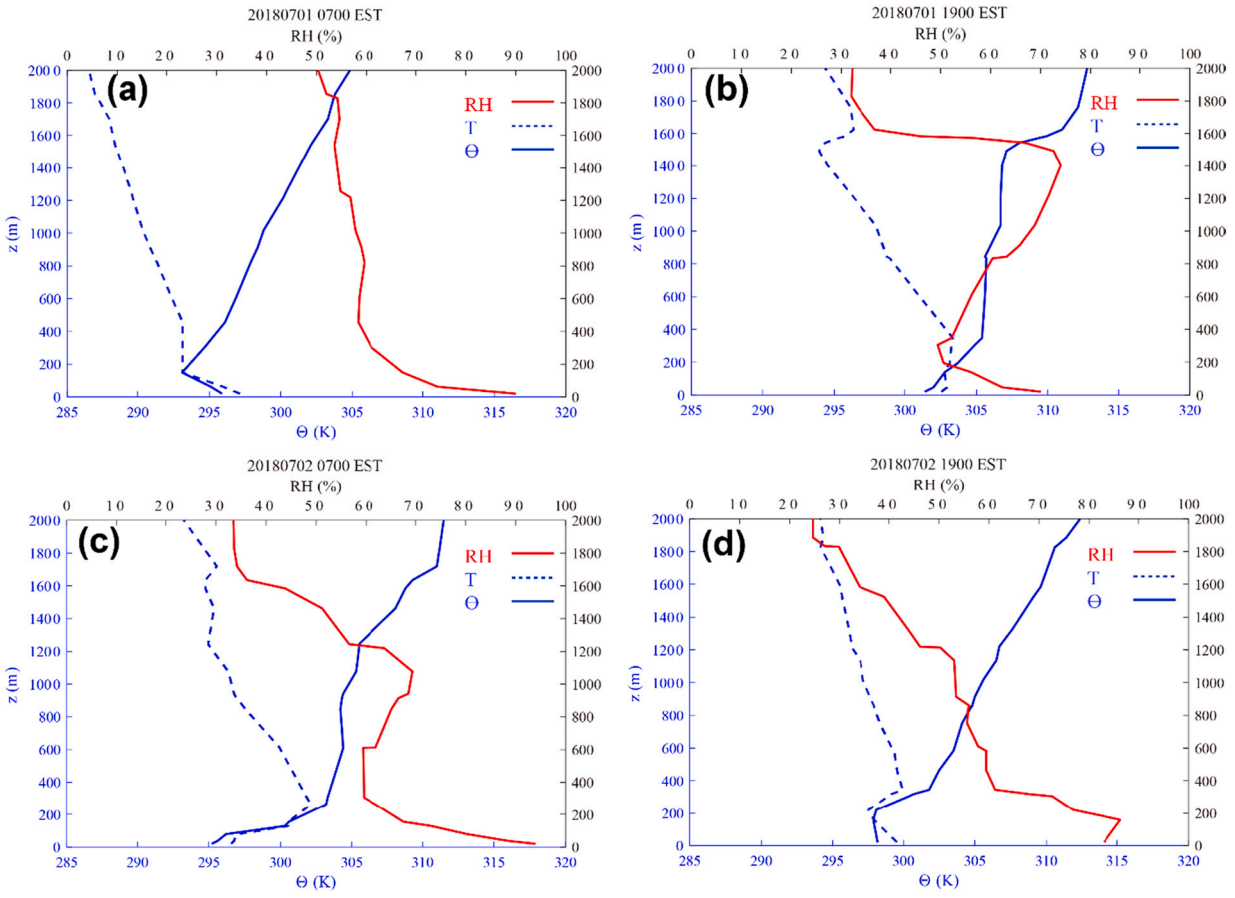

Fig. 4. NWS OKX profiles of RH (%, red), T (K, dashed blue), and θ (K, solid blue) at (a) 0700 and (b) 1900 EST on 1 July and at (c) 0700 and (d) 1900 EST on 2 July. (For interpretation of the references to colour in this figure legend, the reader is referred to the web version of this article.)

(Fig. 2a) show regional high values with a peak just west of NYC. By the next day (Fig. 2b) the peak is south of the City, with a slightly increased maximum (20.0 vs. 20.5 °C).

NARR sea level pressures on 1 July at 1300 EST (Fig. 2c) show a regional warm-core coastal low (L) northeast of NYC, which thus weakens with height becoming a 850 hPa ridge (Fig. 2a). On the O_3 episode afternoon (Fig. 2d), the City is dominated by an offshore H to its west. The concurrent surface flow over NYC on 1 July is southwesterly (alongshore), but by the episode day, it has shifted to a southeasterly (onshore) flow over the City in association with the offshore H. The area northwest of the City, however, is still dominated by a southwesterly (along shore) flow. Concurrent surface T-values on 1 July (Fig. 2c) are relatively low over NYC, with warmer bands northwest and southwest of the City. On the episode afternoon (Fig. 2d), the pattern is similar, but the peak values over the southern NJ hot spot have increased to 36 °C, while those over the City have only increased from 31.0 to 31.5 °C. The NYC NWS Regional Office declares a heat wave with three or more consecutive days with maximum surface temperatures >32.2 °C (90 °F). This threshold is exceeded in these synoptic distributions (Figs. 2c and d) over NJ, but not over NYC. The local scale values discussed below, however, will show that it was in fact exceeded over the City.

The daily surface O_3 AQI values on 1 July, the day before the episode, indicate "unhealthy for sensitive groups" levels over the eastern half of the current outer domain (Fig. 3a), with a smaller area of "unhealthy for general populations" air over western NYC in the current inner domain. On the episode day (Fig. 3b), levels are generally higher, with a greatly expanded "unhealthy" area west of the City, and even a small area of its highest level (very unhealthy for general populations) air north of the inner NYC domain.

The NWS θ-profile at 0700 EST on 1 July (Fig. 4a) shows a super-adiabatic surface layer (4 °C from the surface to 150 m). Fog should have existed near the surface at this time, given the 90% RH in that layer. By 1900 EST (Fig. 4b), the T-profile showed a weak (1 °C to 400 m) surface-based inversion and a weak regional subsidence inversion of 2 °C between 1450 and 1600 m. This weakness is expected, given the associated Hs of Fig. 2 are not directly over NYC. The corresponding RH profile shows the effect of the elevated inversion, i.e., a dramatic decrease of values above its base. The high RH values at 1400 m were probably associated with cloud formation. The 0700 EST T-sounding on 2 July (Fig. 4c) showed a deep surface inversion (7 °C to 300 m) and now only an ill-defined

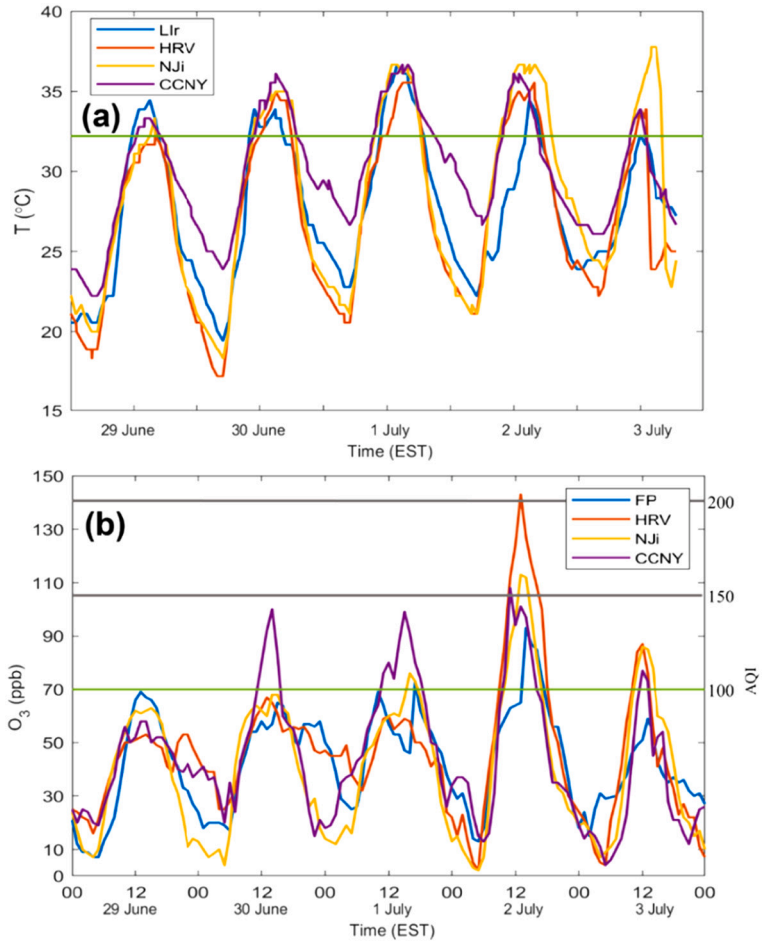

Fig. 5. Observed surface (a) temperatures T and (b) O_3 concentrations for 29 June to 3 July at selected sites. The horizontal line in (a) is NYC hourly heat wave criteria (32.2 °C = 90 °F), while those in (b) represent the EPA 8-h O_3 criteria (70 ppb), as well as 1.5 and twice that value; also shown are corresponding AQI values. All site acronyms are defined in Appendix and located in Fig. 1c.

subsidence inversion (1 °C from 1200 to 1700 m). Even though the subsidence inversion is now weakened, it again corresponds to the base of a low RH layer. By the episode afternoon (Fig. 4d), the θ-profile showed a shallow super-adiabatic surface layer (1 °C to 200 m), while the T-profile showed an elevated inversion of 2.5 °C, but only between 200 and 400 m (discussed below). The sub-inversion RH increase of 30% in the layer between 0 and 200 m is due to its T-decrease.

Surface-T values (Fig. 5a) at four key sites (located in Fig. 1c) with the observed O_3 maxima (discussed below) all peaked midday on 1 July (Fig. 5a), and all showed the three required consecutive days with values above the NYC NWS heat wave criteria of 32.2 °C. The heat wave ended during the night of 2–3 July when rain entered the area. Nighttime minima at all sites were 4 °C higher, starting during the night of 30 June-1 July, due to subsidence-induced adiabatic warming from the synoptic H. The lack of nocturnal relief exacerbated human health impacts from the heat wave. The corresponding surface O_3 time series (Fig. 5b) replaces the LIr site with the nearby Flax Pond site (located in Fig. 1c). The CCNY site first exceeded the EPA 8-h standard of 70 ppb on 30 June due to its normally high rate/concentration of precursor NO_2 emissions. All four sites did so on the episode day of 2 July, with values at HRV reaching 143 ppb (more than twice the "very unhealthy for general populations" trigger level). All sites generally had near-zero nocturnal concentrations due to titration processes. As the O_3 episode occurred only several days after the heat wave onset, it was necessary but not sufficient to trigger the episode.

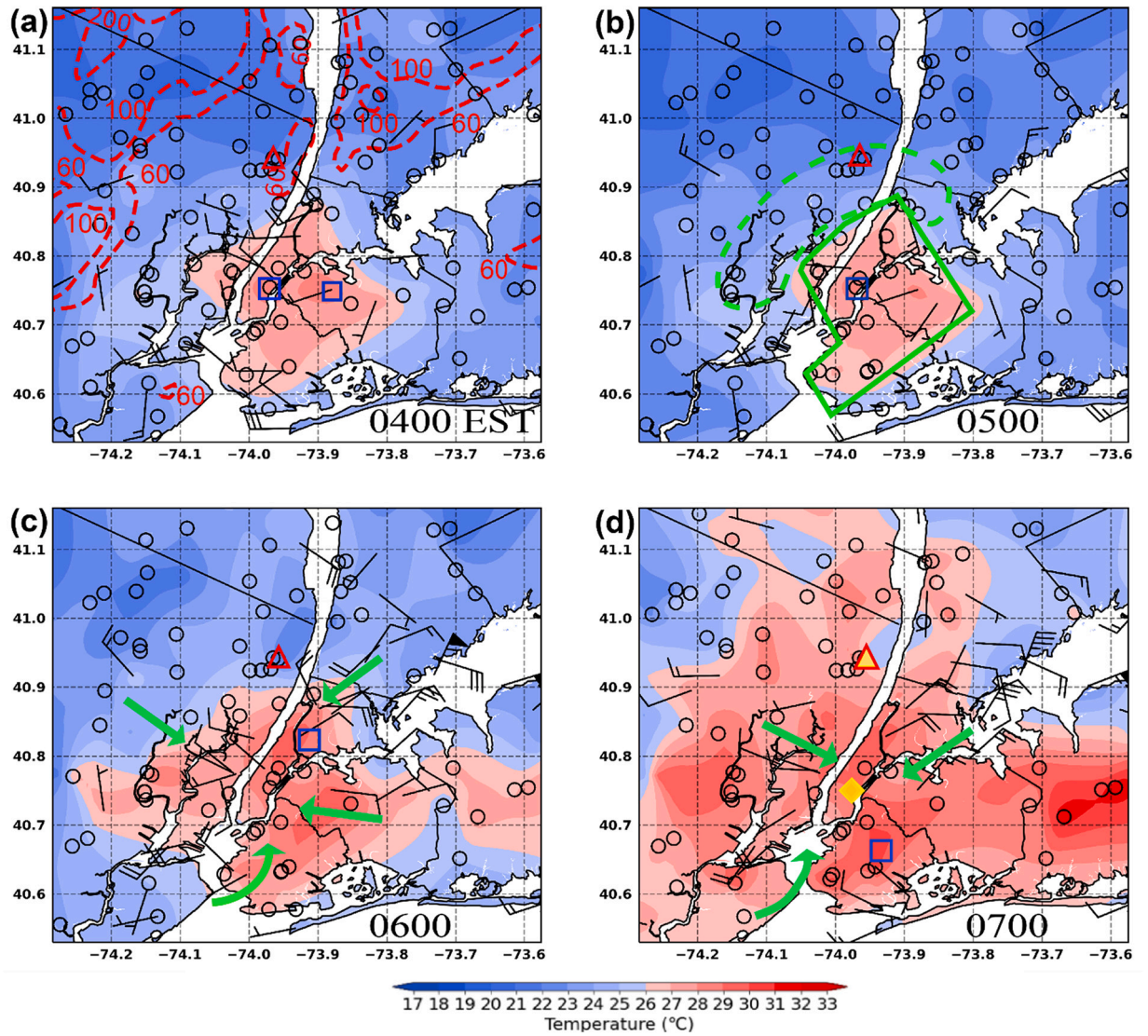

Fig. 6. Hourly surface temperatures (°C, colors) and wind vectors (1 full barb is 1 m/s, circles indicate calm) in and around NYC on 2 July at (a) 0400, (b) 0500, (c) 0600, and (d) 0700 EST, while green arrows represent subjectively located area-average flows. Panel (b) shows the urban and rural areas of Fig. 1b for UHI calculations (solid and dashed green outlines, respectively). Also shown are key topographic heights (m, red lines) and sites with *hourly* maximum (□) and minimum (△) temperatures, as well as those with maximum (◆) and minimum (▲) *averages* over a 5-h period. (For interpretation of the references to colour in this figure legend, the reader is referred to the web version of this article.)

In summary, synoptic conditions on 1–2 July were dominated by a high-pressure ridge centered northeast of NYC. Concurrent surface flows over the City changed from along shore on 1 July to onshore on the episode day, while surface T-values on both days showed a regional heat wave event. Such conditions in coastal areas are conducive to SBF formation and to strong regional photochemical activity.

3.2. Inner domain nocturnal UHI and NO_2 values

Nocturnal surface T-values over NYC on the episode day of 2 July at 0300 EST (not shown) and 0400 EST (Fig. 6a) show the warmest areas (for display convenience, arbitrarily defined as ≥26 °C) centered over its four northern boroughs (all except Staten Island). Not much changed during the next hour (Fig. 6b) as maximum values remained constant. By 0600 EST (Fig. 6c), however, the warm area has extended westward into NJ and eastward into LI, while maximum NYC values have increased by 1 °C. An hour later, the more rapid solar warming of the less urbanized areas surrounding the City almost masked its UHI (Fig. 6d). Such differential morning warming is characteristic of adjacent urban and suburban areas (Imamura, 1991; Bornstein et al., 2012; Oke et al., 2017).

Specific values at 0300 EST showed the warmest urban and coolest rural sites as 29.4 and 22.2 °C, respectively, and thus the UHI was 7.2 °C. By 0400 EST the UHI value was unchanged, as both sites cooled by 0.5 °C. During both hours, the same NJ site was the

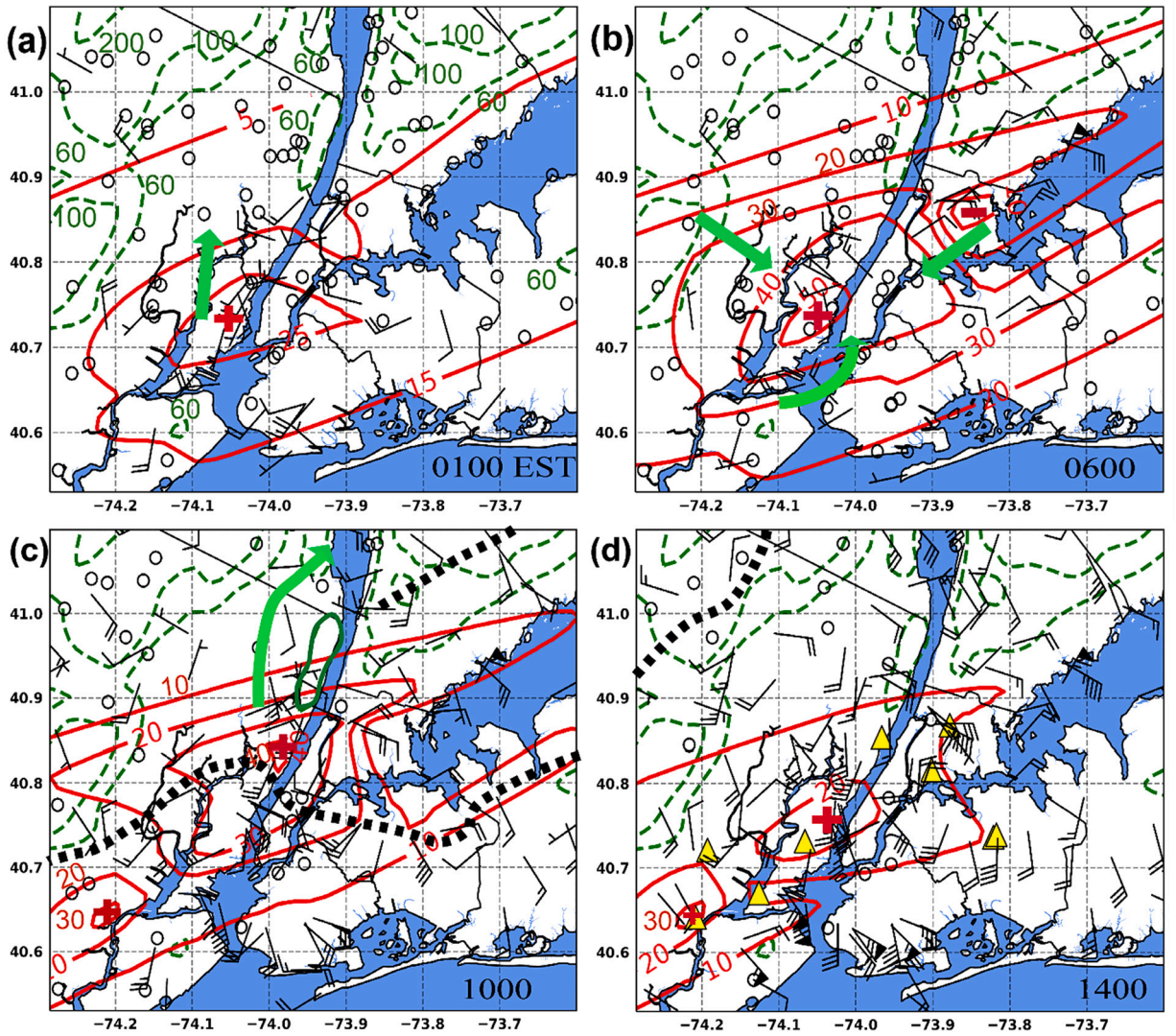

Fig. 7. Surface NO_2 concentration (ppb, red lines) and wind vectors (1 full barb is 1 m/s, circles indicate calm) in and around NYC on 2 July at (a) 0100, (b) 0600, (c) 1000, and (d) 1400 EST. Also indicated are local NO_2 maxima (+), NO_2 sites (▲), subjectively placed area-averaged flow directions (green arrows), and sea breeze frontal positions (black dashed lines). (For interpretation of the references to colour in this figure legend, the reader is referred to the web version of this article.)

coolest (Fig. 6a), while a Manhattan and a Queens site both had the same maximum. While the extreme values at 0500 EST were unchanged, the (now) single warmest urban site was in Manhattan (Fig. 6b), while the coolest rural one was unchanged. By 0600 EST the urban site had warmed by 1.1 °C while the rural site remained the same, and thus the UHI increased to its maximum of 8.3 °C (Fig. 6c). The location of the warmest urban site had moved from Manhattan to The Bronx, while the coolest NJ rural site had moved slightly eastward. One hour later the rural site had again warmed faster and thus the UHI had again decreased to 6.7 °C. The average UHI value over the period was 7.3 °C. The UHI peaks at 0600 and 0700 EST induced a clearly discernable convergence over NYC into its associated thermal L (Figs. 6c and d).

Surface winds in and around NYC at 0100 EST on 2 July (Fig. 7a) show mostly calm conditions north and west of the City. Photochemical precursor NO_2 concentrations are maximum (30 ppb) just west of NYC, extending eastward into Brooklyn. The concurrent weak local northward flow in NJ (and the next four hours) could impact the future O_3 peak north of NYC (discussed below). By 0600 EST (Fig. 7b) the UHI convergence (of Fig. 6c) has increased the NO_2 to its maximum value (about 50 ppb) due to containment of its rush hour emissions. Four hours later (Fig. 7c), the post-rush hour peak has decreased to 40 ppb and its location has been pushed northward ahead of the incoming "Ocean" SBF, which came onshore about 0700 EST (panel not shown). The western edge of a second SBF, the "Connecticut" front from LI Sound, is also seen at this time; both SBFs will be discussed in detail in the following figure. The NO_2 peak was then apparently transported around the western edge of the NJ Palisades and then northward into the HRV. Its photochemical conversion along this trajectory would thus explain the observed HRV O_3 peak at 1300 EST (discussed below). By 1400 EST (Fig. 7d) the SBFs had passed NYC, and the NO_2 maximum has further decreased to 20 ppb as new emissions are advected out of NYC by the post-frontal onshore flow.

In summary, given the limited NO_2 observations network, the fate of its pre-SBF emissions is unknowable from just this data. It seems, however, that early morning precursor pollutants were drifted into a calm area in NJ by a weak westerly regional flow, before the latter emission became trapped in the UHI-induced convergent flow into NYC. Late morning emissions were once again pushed, this time by the SBF, into NJ and northward around the Palisades into the HRV.

3.3. Outer domain heat wave, SBFs, NO_2, and O_3

Two SBFs that formed from flows from the LI Sound were first seen at 0700 EST (Fig. 8a), i.e., the Connecticut front (seen 3-h later in Fig. 7c) along its southern coast and a short-lived "Northern LI" front. The separate Ocean front (also seen 3-h later in Fig. 7c) along the southern LI and NYC coasts here is seen to follow the shape of Jamaica Bay. All three fronts brought speed increases of up to 4–6 m/s when they came onshore. One hour later (Fig. 8b), the Connecticut front had moved further onshore, with speed increases of another 2–3 m/s. The Ocean and Northern LI fronts, however, showed less movement due to blockage by the local topographic features in

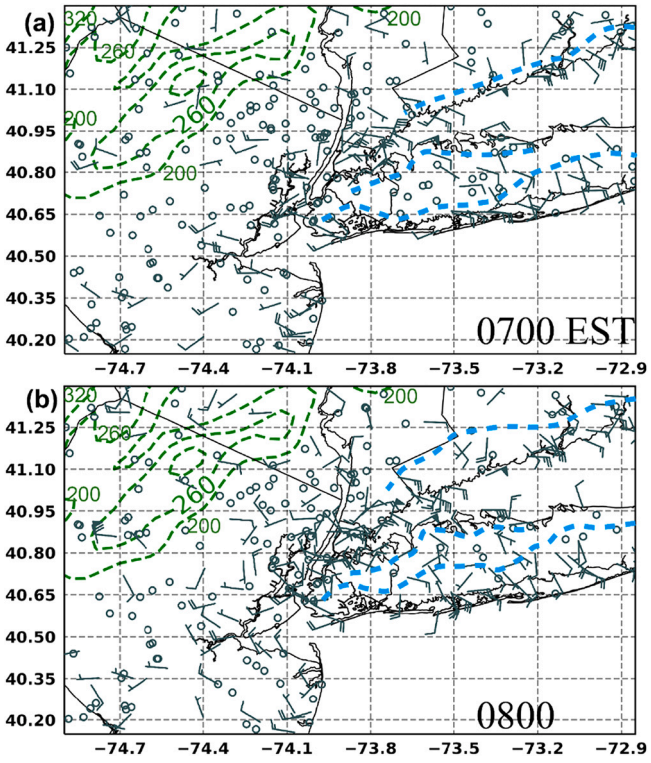

Fig. 8. Wind vectors (1 full barb is 1 m/s, circles indicate calm) on 2 July at (a) 0700 and (b) 0800 EST, with subjectively placed sea breeze frontal positions (blue lines). (For interpretation of the references to colour in this figure legend, the reader is referred to the web version of this article.)

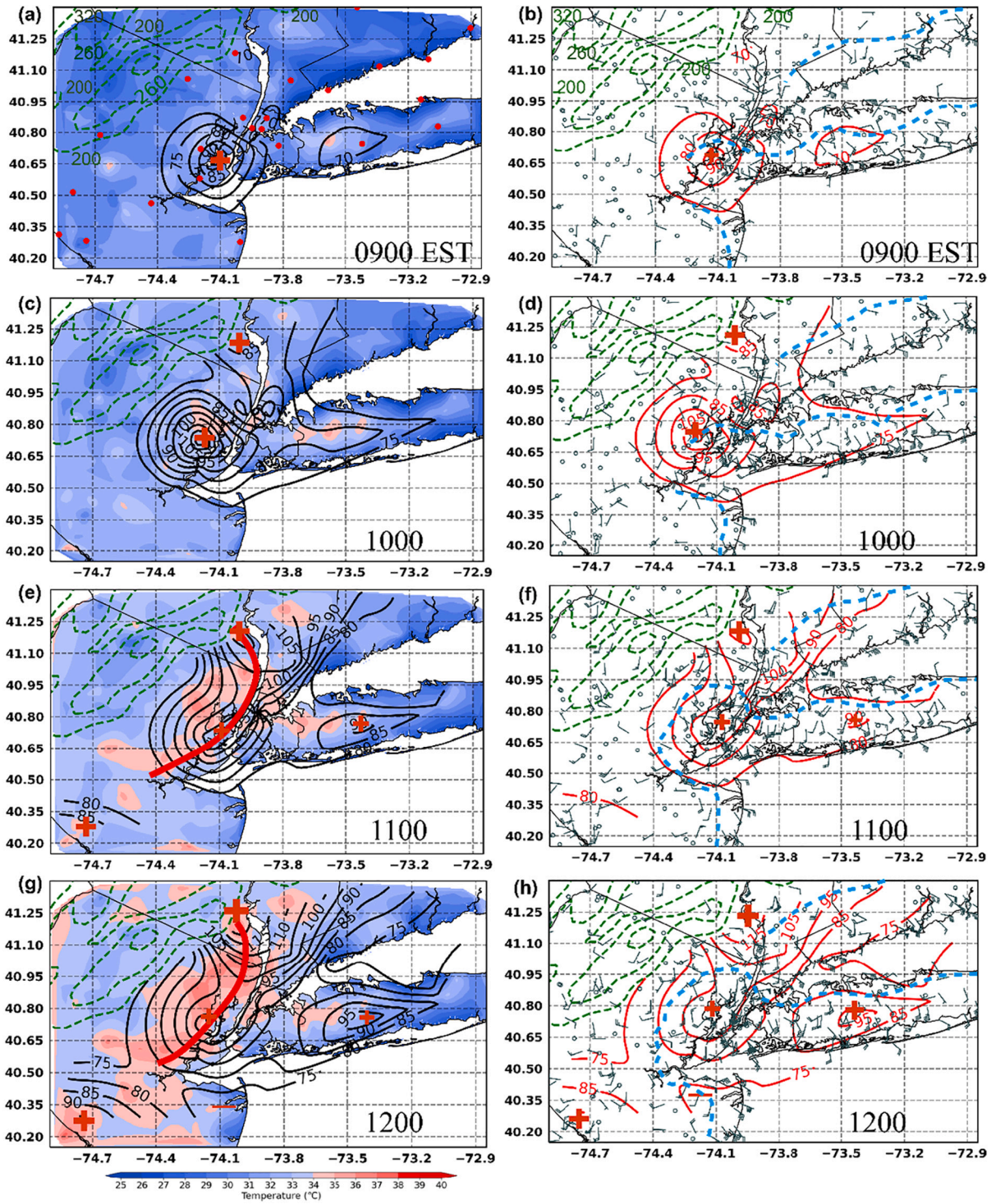

Fig. 9. Contours of high (≥ 70 ppb) surface O_3 concentration (ppb, black lines), their local maxima (+) and minima (-), and temperatures (°C, colors) on 2 July at (a) 0900, (c) 1000, (e) 1100, and (g) 1200 EST. Concurrent wind vectors (1 full barb is 1 m/s) and O_3 concentrations (ppb, red lines) are shown in (b), (d), (f), and (h), respectively, along with subjectively placed: sea breeze frontal positions (blue) and maxima O_3 ridge lines (red). (For interpretation of the references to colour in this figure legend, the reader is referred to the web version of this article.)

Fig. 1.

Surface T-values 1-h later (0900 EST, Fig. 9a) show that the regional warming of 5 °C during the two hours since Fig. 6d has produced near-uniform values with little evidence of a UHI. The concurrent photochemical O_3 maximum of 90 ppb (first one >70 ppb) exists just west of NYC (site NJm in Fig. 1c), co-located with the NO_2 maximum of Fig. 7c. The O_3 peak is higher than the 8-h EPA standard of 70 ppb. The Ocean front (Fig. 9b), here1-h earlier than its position in Fig. 7c, has now merged with and absorbed the Northern LI front of Fig. 8. Its maximum penetration is downwind of the northern edge of the NY Bight, a western extension of the Atlantic. It has also moved northward over LI and the mostly residential Brooklyn and has arrived at southern Manhattan (collocated with the O_3 peak); a new southern segment has formed along the eastern NJ coast.

By 1000 EST (Fig. 9c), a local warm spot (>35 °C) appears just northeast of the New Jersey maximum (NJm) O_3 maximum, which has increased to 110 ppb. Local communities were now thus in areas above the NYC heat wave warning of 32.2 °C and within the EPA AQI range of unhealthy for sensitive groups. A small new peak of 85 ppb has also formed at the HRV site, perhaps due to photochemical conversion of the early morning northward advected NO_2 emissions of Fig. 7a. A weaker O_3 peak has also formed over central LI; all maxima are associated with local T-peaks. All SBF segments have concurrently moved slightly inland (Fig. 9d), except for those over coastal NJ and Manhattan, which have stalled against the coastal hills and building topography, respectively; post-frontal speeds have once again increased by 1–3 m/s. The Ocean front still coincides with the main NJm O_3 maximum, whose center has been advected

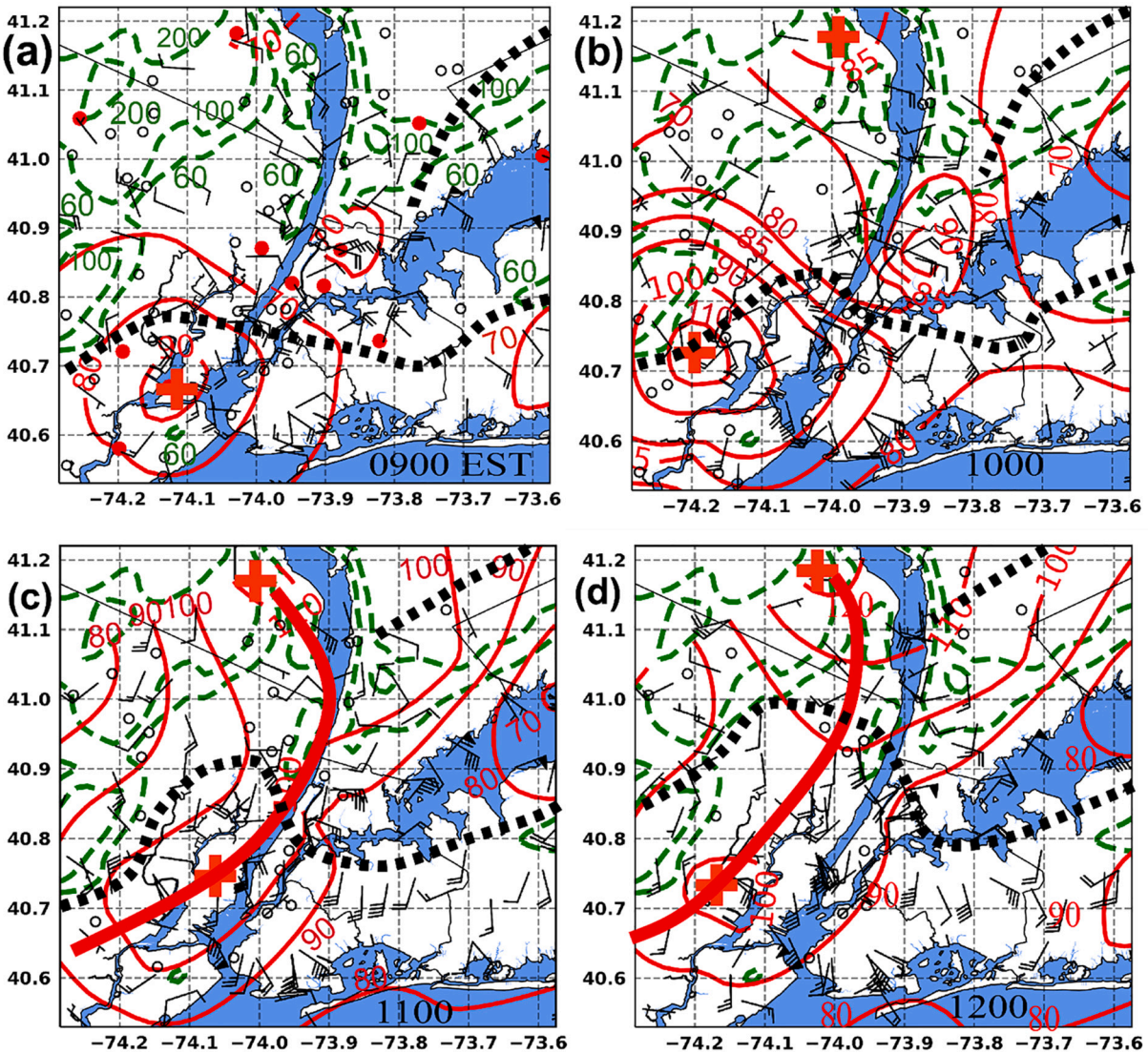

Fig. 10. Contours of high (≥ 70 ppb) surface O_3 concentration (ppb, thin red lines) in inner domain, their local maxima (+), O_3 sites (red dots), and wind barbs (1 full barb is 1 m/s) on 2 July at (a) 0900, (b) 1000, (c) 1100, and (d) 1200 EST. Also shown are subjectively placed sea breeze frontal positions (black dashed lines) and O_3 ridge lines (thick red lines). (For interpretation of the references to colour in this figure legend, the reader is referred to the web version of this article.)

further inland by its post-frontal winds; the Connecticut front is still southeast of the HRV O_3 peak.

An hour later (Fig. 9e) at 1100 EST, regional warming has increased T values by another 1 °C at the now many local hot spots in NJ, NYC, and LI. While the HRV O_3 peak is now the largest (at 110 ppb, now unhealthy for all populations), the local NJm O_3 peak has decreased slightly to 105 ppb; a subjectively placed "ridge line" has been placed to connect the two maxima. The LI peak has also increased (to 90 ppb), and a new maximum has appeared at the NJ industrial site (NJi); all peaks are still associated with a local T hot

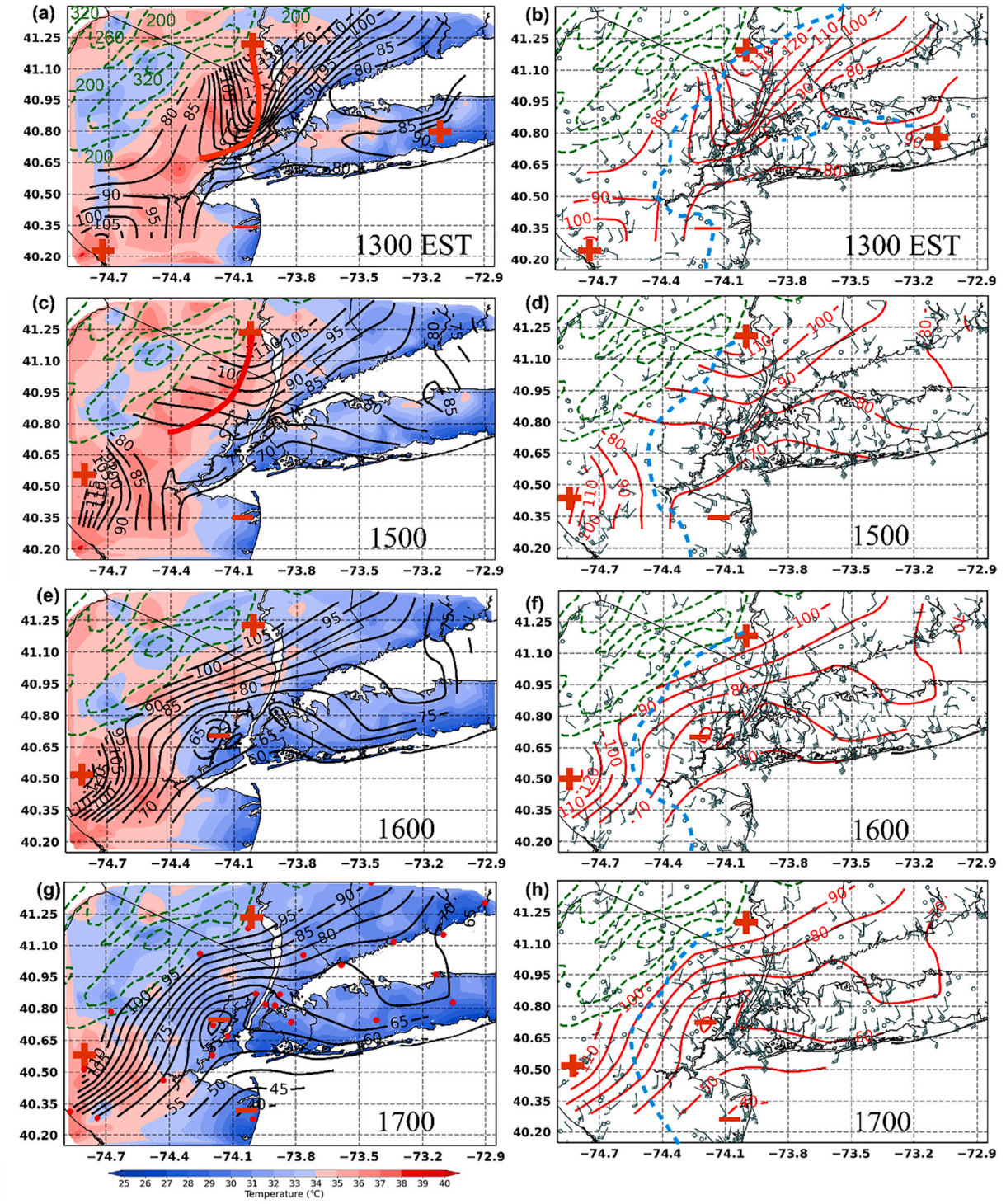

Fig. 11. As in Fig. 9, but in (a) and (b) at 1300; (c) and (d) at 1500; (e) and (f) at 1600; and (g) and (h) at 1700 EST.

spot. Inland SBF penetration has again concurrently continued (Fig. 9f), with the Ocean and coastal NJ fronts now having joined into a single "Combined" front, whose shape follows the outline of the NY Bight. While its segment over LI continues to now move only slowly northward, as it approaches the hills in that area (in Fig. 1), that over central Manhattan is even more distorted by its buildings, consistent with Bornstein and Thompson (1981) and Novak and Colle (2006). While the Connecticut front is approaching the HRV O_3 peak, the Combined front has moved ahead of the NJm peak and its cooler marine air has slowed the photochemistry, producing decreasing concentrations.

By 1200 EST (Fig. 9g) the NJ T-hot spots have merged into an almost continuous northeast to a southwest band of high values, with some pre-frontal locations now >38 °C and with post-frontal values over NYC and LI <36 °C. The O_3 ridge line has moved slightly westward and now collocates with the high-T band. Three of the four O_3 peaks show increased values, while NJm values continue to decrease. The highest (120 ppb) is at HRV, with the other two within 90 to 100 ppb. As the LI peak is clearly separated from the NJ O_3 ridge line, it will be discussed in the following section. While the LI segment of the Combined SBF (Fig. 9h) has continued its slow northward movement, its segment over NYC has now rapidly passed Manhattan. While the Connecticut front is now somewhat closer to the HRV peak, the O_3 ridge line is further behind the Combined front. Such a high O_3 concentration band behind a moving SBF was first observed by Gaza (1998) for the Connecticut SBF and then by Hy-Eun et al. (2013) on the Korean coast. The current effort seems to be the first to show it downwind of a major urban area and impact its movement. It also seems first to identify an O_3 maximum in the HRV, although Zhang et al. (1998) did report a river valley effect in Connecticut.

Finer details of NYC impacts on SBF penetration and of its relationship with the NJm high O_3 concentrations can again best be seen in the inner domain patterns. At 0900 EST (Fig. 10a) the Ocean front is only a bit distorted over the City. An hour later (Fig. 10b), the front is more distorted over NYC, as it has moved only slightly northward over Manhattan, while the segment over the NY Bight penetrates more rapidly; the 1100 EST locations (Fig. 10c) shows still further distortions. After an additional hour (Fig. 10d), however,

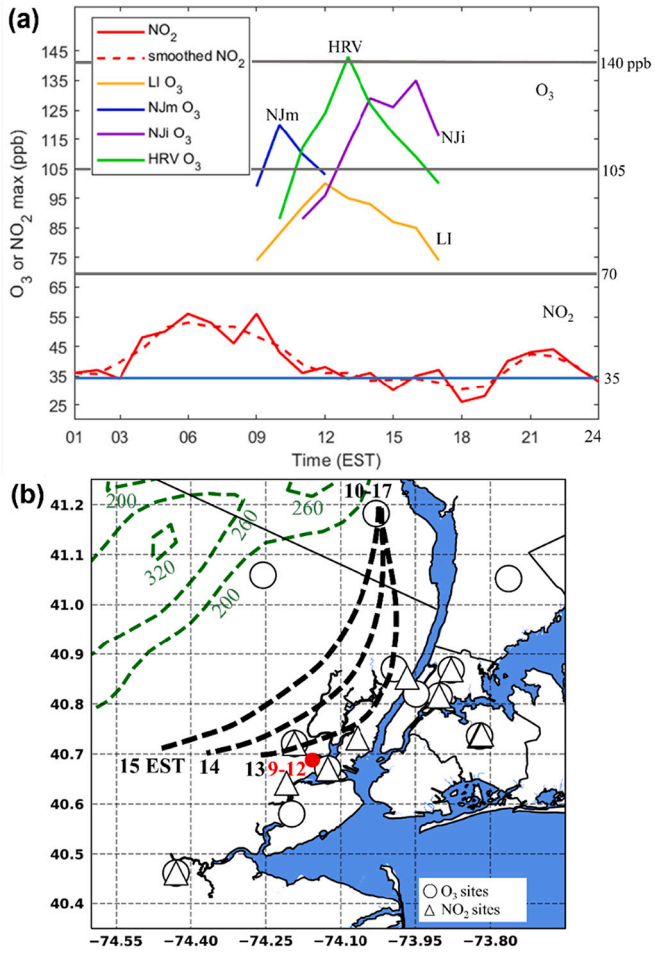

Fig. 12. Overserved (a) surface peak NO_2 (red) and O_3 at the LI **(orange),** NJm (blue), NJi (purple), and HRV (green) sites in Fig. 1c for 2 July. Horizontal lines are the EPA eight-hour O_3 criteria (and 1.5 and twice that value) and NO_2 background concentration. Panel (b) shows the O_3 maximum site at 0900–1200 EST (●), subsequent peak value ridge lines (black dashed), as well as NO_2 (□) and O_3 (○) sites. (For interpretation of the references to colour in this figure legend, the reader is referred to the web version of this article.)

the front has finally passed Manhattan, but the distortion has still grown as the segment over NJ continued its even more rapid northward movement. These hourly frontal positions relative to the NJm O_3 maximum can also be seen in the panels, i.e., the SBF starts close to the maximum, but as it moves further northward, the peak remains localized. The SBF locations in Fig. 9 could not detail these distortions. They were also not seen in Bornstein and Thompson (1981) as they lacked the current station density, but they were seen in the Novak and Colle (2006) zoom-ins.

Outer domain maximum T-values an hour later (1300 EST, Fig. 11a) are 1 °C higher than in the preceding hour (Fig. 9g) over most of NJ, except for its western hilltops. In the post-frontal flow over NYC and LI, values are still <36 °C. The local NJi O_3 peak has increased to 105 ppb, while the local LIr peak has moved eastward towards Flax Pond and started to decrease. The NJm and HRV O_3 peaks have combined, producing an absolute peak near the northern site, while the O_3 ridge line has kept moving slowly westward. The combined 143-ppb value is the highest of the episode and is just above the lower limit for the direst EPA warning: very unhealthy for all populations with a measured AQI value of 204. This health impact is compounded in much of the area by the simultaneous heat wave. The concurrent Connecticut front (Fig. 11b) has continued northward and has merged with the NJ section of the Combined (Ocean and coastal NJ) front to form a "Regional front," which coincides with the HRV O_3 peak. The now separate LI frontal segment has moved to its northern coast and is not seen again subsequently.

By 1500 EST (2-h later, Fig. 11c) peak T-values (still >39 °C) over NJ have maximized both in areal coverage and north-south extent but have narrowed somewhat in the east-west direction. While coastal values have fallen to <34 °C, they still are above the NYC heat wave criteria. The O_3 ridge line has continued westward, with its single maximum at HRV now decreased by 25 ppb (to 120 ppb) due to reduced late afternoon regional photochemical activity; this value is still within the EPA unhealth for all very populations range with an AQI value of 171. The separate NJi O_3 peak has moved slightly northwesterly and increased by another 15 ppb (to 120 ppb), while the LIr peak is no longer visible. The (sole remaining) Regional SBF (Fig. 11d) has moved westward along its entire length and it now coincides with the band of maximum T-values. While its coastal NJ segment has finally moved rapidly inland, it has not reached the NJi site where O_3 concentrations have continued to increase. Post-frontal coastal areas contain the cooler T-values, a southeasterly flow, and the trailing O_3 ridge.

An hour later (Fig. 11e) peak T-values have finally cooled to 38 °C, but still way above the NYC heat wave criteria. A clear coastal O_3 minimum of 60 ppb has formed, and the O_3 ridge is no longer evident as it has been replaced by a "band" of high values with a strong gradient directed to the northwest. While the HRV peak has continued to decrease to 105 ppb, the NJi value has peaked at 125 ppb. These two sites are at the western edge of the O_3 network, so concentration lines cannot be drawn into the western hills. The concurrent northern segment of the Regional frontal (Fig. 11f) has continued to move into the hills, a region with more meteorological than O_3 sites (Fig. 1). By 1700 EST (Fig. 11g) uniformly cool T-values exist throughout the domain, except its southwest corner. The O_3 band has grown to encompass the NJi peak, and values there have finally decreased. Two maxima still exist, i.e., >110 and 95 ppb at the southern and northern locations, respectively, and the coastal minimum has decreased by another 10 ppb. While the concurrent Regional front is still moving westward (Fig. 11h), it has yet to reach the NJi site. A frontal position could not be determined after 1800 EST (not shown).

3.4. Episode summary

A summary time-series plot of episode values on 2 July around NYC (Fig. 12a) shows peak hourly surface NO_2 values with a nocturnal background residual of about 35 ppb until 0300 EST. The slow increase to about 55 ppb over the next 3-h was due to home energy use and automotive rush hour emissions trapped by the UHI-induced convergence of Fig. 7b. The resulting near-constant peak lasted until 0900 EST and was followed by a rapid 2-h decrease to the background value due to O_3 photochemical conversion processes. Values remained low until 1800 EST, when reduced insolation and late afternoon rush hour traffic produced a peak of 45 ppb at 2200 EST, a value below the early morning peak. A similar plot of high O_3 values at four key areas shows the earliest local maximum (120 ppb, unhealthy for all populations) at 1000 EST near NJm, west of NYC. This peak arose from photochemical conversion of the nearby 0900 EST NO_2 peak, and then decreased by advection as the Ocean front passed. The LI peak occurred 2-h after the first maximum,

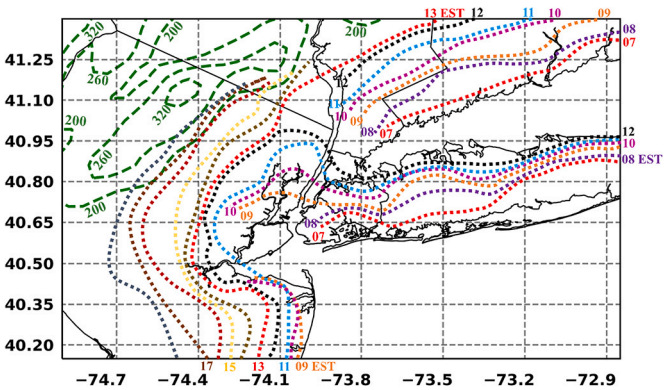

Fig. 13. Hourly 2 July sea breeze front locations during 0700–1800 EST; short-lived Northern LI front not shown.

with a lower value (100 ppb) from a recirculated air mass (discussed below) and then decreased as the Ocean front passed. The (episode) peak at HRV (145 ppb that occurred yet another hour later at 1300 EST arose from northward transport of pre-frontal NO_2 emissions (discussed in next section). The latest O_3 peaks near NJi at 1400 and 1600 EST (127 and 135 ppb, respectively) were due to local industrial emissions.

A spatial summary of the above O_3 results (Fig. 12b) focuses on NYC impacts and thus omits the discussion of the LI and NJi peaks. The NJm peak first appeared southwest of NYC at 0900 EST and remained localized until 1200 EST. The HRV peak was first seen at

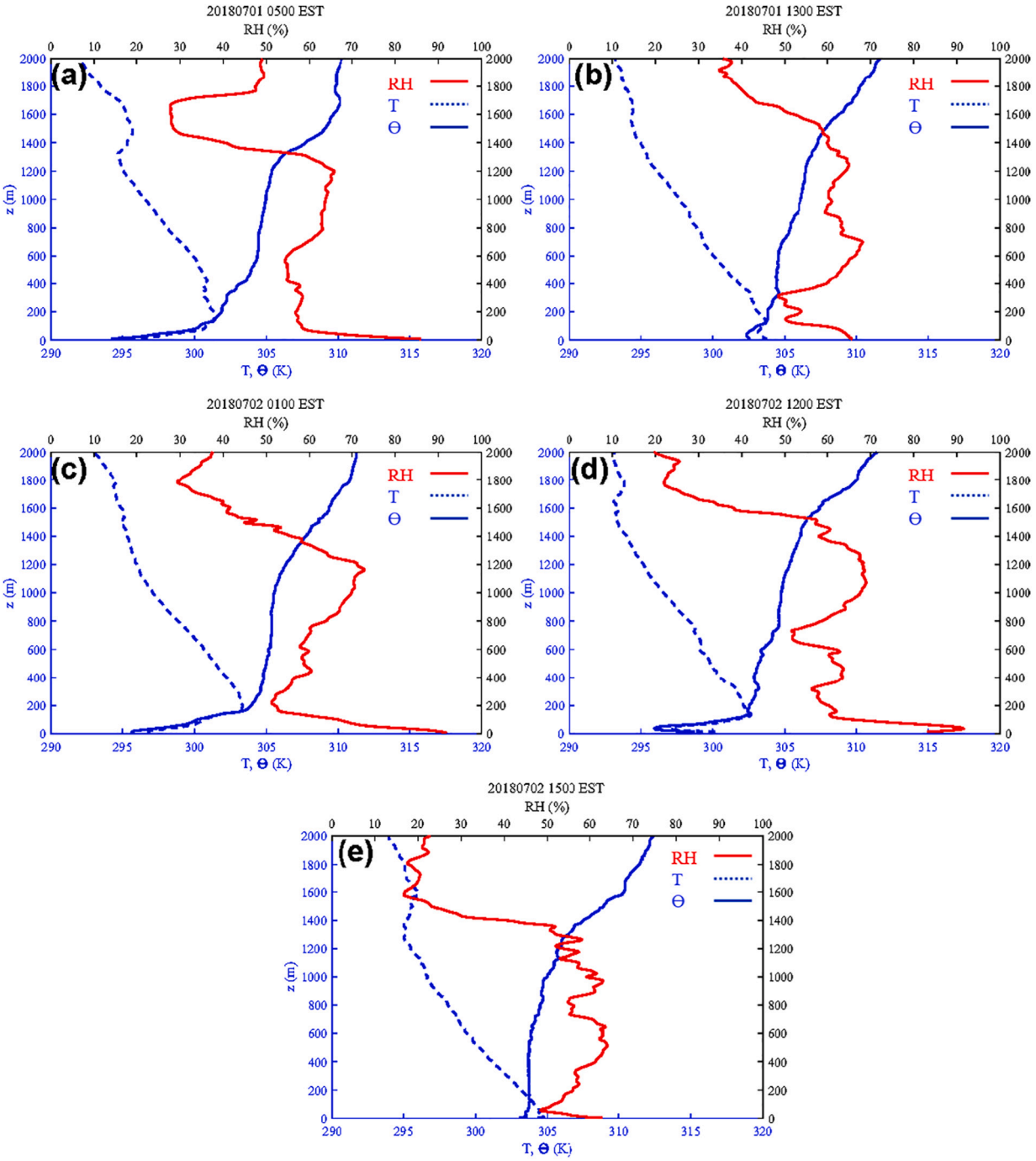

Fig. 14. Vertical profiles at Flax Pond of RH (%, red), T (K, dashed blue), and Θ (K, solid blue) at (a) 0500 and (b) 1300 EST on 1 July and at (c) 0100, (d) 1200, and (e) 1500 EST on 2 July. (For interpretation of the references to colour in this figure legend, the reader is referred to the web version of this article.)

1000 EST and remained at this site (only one in area) until 1700 EST. These independent peaks lay along a single ridge of high values at 1100 EST, and combined as the ridge moved further into NJ during the next 2-h. After 1500 EST, the O_3 from NYC area NO_2 emissions could no longer be differentiated from that in the regional O_3 episode to the west. This study is the first to identify an O_3 maximum in the HRV, which seems to have arisen first from northward-transported early morning precursor emissions, before they were cut off by a UHI-induced convergence into NYC, and then from post-SBF precursors emissions transported northward around the NJ Palisades into the HRV. Tri-state area (NY, NJ, and Connecticut) air quality networks focus on coastal pollutants and have fewer inland sites. The current effort has identified areas with too few sites, i.e., north of NYC for NO_2, north of the HRV site, and near the NJ hills for O_3.

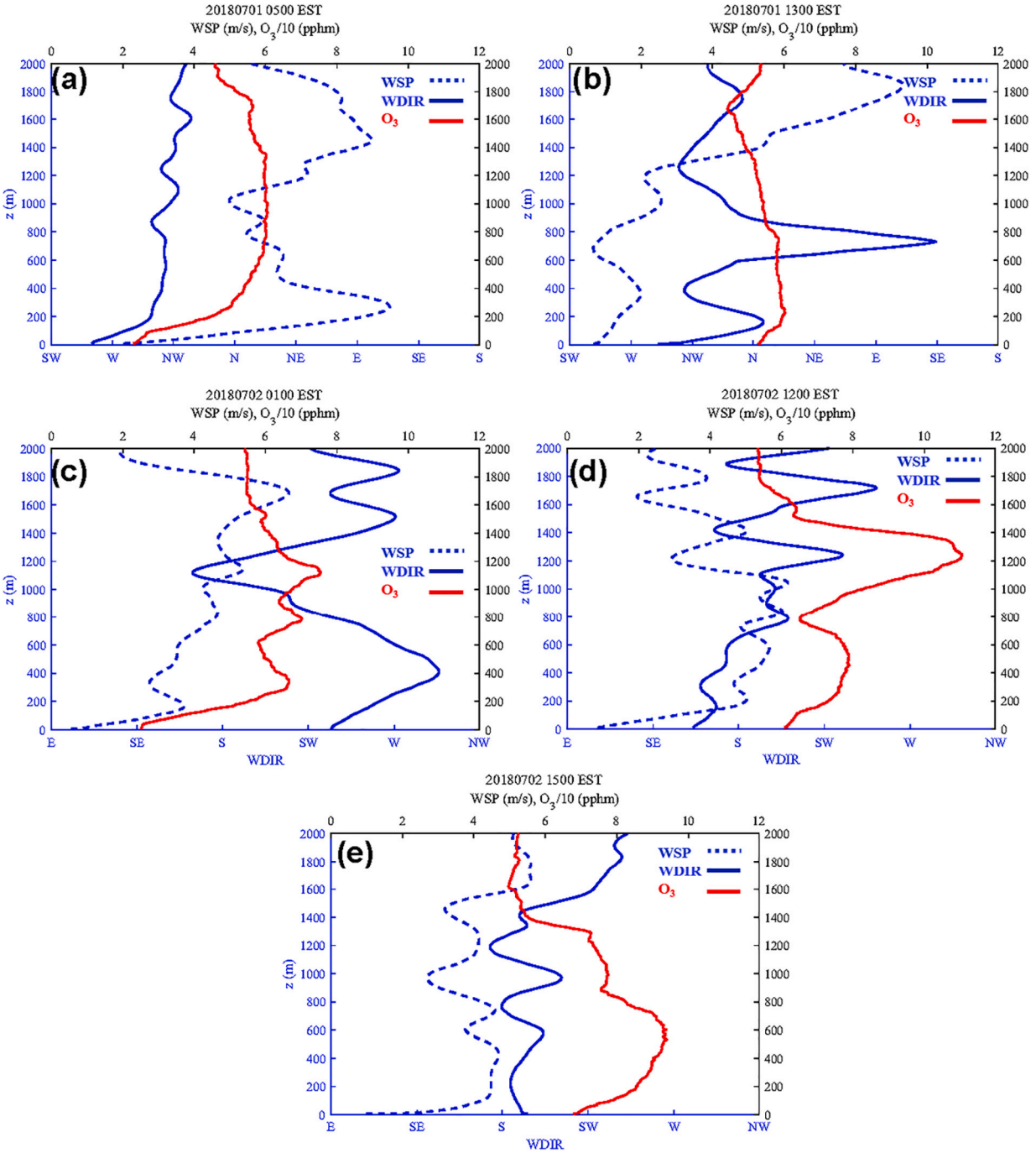

Fig. 15. Vertical profiles at Flax Pond of ppb O_3 divided by 10 (pphm, red), wind speed (m/s, dashed blue), and wind direction (solid blue) at (a) 0500 and (b) 1300 EST on 1 July and at (c) 0100, (d) 1200, and (e) 1500 EST on 2 July. (For interpretation of the references to colour in this figure legend, the reader is referred to the web version of this article.)

A summary of all hourly SBF positions (except for the short-lived North LI front) shows that they came ashore at 0700 EST (Fig. 13), were distorted by Jamaica Bay and the NY Bight, retarded over Manhattan, and combined into a single Regional front, which could be tracked inland until 1800 EST. This pattern is more realistic than the idealized one shown by Bornstein and Thompson (1981), which had the fronts crossing the Bight and Jamaica Bay. The early appearance of the Ocean SBF over the NYC boroughs of Brooklyn and Queens was probably aided by the still extant UHI, which strengthened the existing land-sea T-gradient.

3.5. Flax pond PBL ozone

The LISTOS 0500 EST ozonesonde T-profile at Flax Pond on 1 July (Fig. 14a) shows a deep nocturnal surface-based radiative inversion (8 °C over 200 m) and a weak elevated regional subsidence inversion (2 °C from 1250 to 1450 m). The corresponding RH profile shows that the subsidence inversion has produced a dramatic RH decrease above its base. By 1300 EST (Fig. 14b) both inversions have weakened, while its corresponding θ-profile shows a shallow super-adiabatic daytime surface layer (1 °C over 50 m). Note that NWS OKX radiosonde at 0700 EST (Fig. 4a) does not show the subsidence inversion, although it is seen at 1900 EST (Fig. 4b). Both Flax Pond soundings, taken 25 km northwest of OKX, thus provided complementary data at times between the NWS soundings.

The 0100 EST sounding on 2 July (Fig. 14c) also shows a deep nocturnal surface inversion (8 °C to 200 m). While a well-defined subsidence inversion is not present, the decreased T-gradient at 1.4 km again corresponds to decreased RH values. By 1200 EST (Fig. 14d), the θ-profile shows a stronger shallow super-adiabatic surface layer (about 2 °C over 50 m), while the subsidence inversion in the T-profile (1 °C from 1600 to 1750 m) is stronger than in the previous two soundings. Its near-surface elevated inversion (7 °C from 50 to 170 m), not seen in the previous daytime T-sounding is discussed below. While 3-h later, the T-profile (Fig. 14e) shows only small changes in the subsidence inversion, it no longer shows either the super-adiabatic layer or the near-surface elevated inversion.

The corresponding Flax Pond wind profiles at 0500 EST (Fig. 15a) on 1 July show a mainly west-northwesterly onshore PBL flow (at this LI north-shore site), with a low-level jet of about 10 m/s at the 200 m level and a similar regional peak at 1500 m. Such a jet had been seen on the south shore of LI by Colle and Novak (2010). The near-surface O_3 minimum of 20 ppb (shown as 2 pphm for convenience of plotting) is probably due to NO_x titration. By 1300 EST (Fig. 15b) the near-surface onshore flow has veered (i.e., shifted clockwise) slightly to a north-northwesterly flow; the strong vertical shear above produces an easterly flow at 700 m. A well-mixed daytime O_3 layer of about 50 ppb is seen throughout the PBL.

The 2 July wind profile at 0100 EST (Fig. 15c) showed that the near-surface flow has backed (i.e., shifted counterclockwise) producing south-southwesterly flow. PBL winds at 1200 m are now south-southeasterly in association with a strong vertical shear. Nighttime near-surface O_3 values are again low and are capped by high values at 200 to 1200 m. By 1200 EST (Fig. 15d) near-surface winds are south-southeasterly, as the NARR surface synoptic flow was changing to this direction (Fig. 2c vs. d). This allowed the Ocean

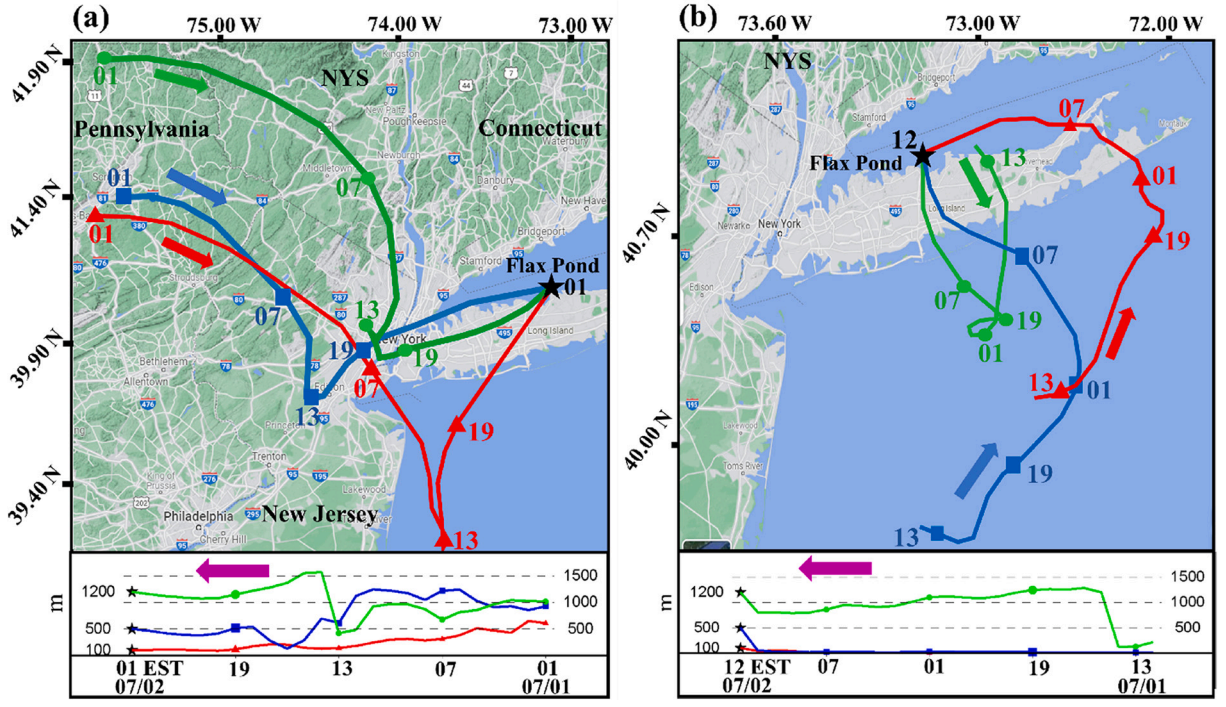

Fig. 16. HYSPLIT back trajectories ending at Flax Pond (*) at (a) 0100 and (b) 1200 EST on 2 July at receptor heights of 100 (red), 500 (blue), and 1200 (green) m AGL. Lower boxes show elevations along each trajectory, with time increasing from right to left **(purple arrow).** (For interpretation of the references to colour in this figure legend, the reader is referred to the web version of this article.)

front to form on the south shore of LI and move northward, while the flow at 1200 m is south-southwesterly, i.e., from NYC. The 1200 EST elevated inversion at 50–170 m in Fig. 14d is probably due to the northward moving elevated "nose" of the Ocean front. While the surface front was still just south of Flax Pond (Fig. 13), the nose should have just passed the site (Simpson, 1994). The near-surface O_3 minimum of about 60 ppb is probably due to daytime dry deposition over this precursor-poor area and is capped by a well-mixed layer of about 80 ppb between 200 and 600 m. The upper-level peak of 110 ppb at 1200 m will be discussed below. Three hours later (Fig. 15e) the wind profiles have not changed, but PBL O_3 values to 1200 m are now generally well mixed and the upper-level peak has decreased by 30 ppb.

Hysplit 24-h back trajectories ending at Flax Pond (Fig. 16a) help to determine the origin of the air that produced its elevated O_3 peak at 0100 EST on 2 July (Fig. 15c). The 1200 m parcel arriving at 0100 EST originated at Pennsylvania (in an area north of NJ) at 1000 m (near the PBL top) on 1 July at 0100 EST. It flowed southeastward within the layer between 750 and 1000 m for about 11 h, then descended to about 500 m in an area west NYC over from 1100 to 1300 LST. Its descent was probably due to downward motion associated with a bifurcating divergent flow around the City, as observed over NYC (Bornstein, 1987a, 1987b) and Beijing (Dou et al., 2015, 2020). From about 1300–1500 EST the air moved slowly over NYC towards the coast, before sharply turning to the northeast. Before the turn, the air quickly rose to 1500 m and then slowly descended to 1200 m. The rise was probably due to upward motion at the backwards sloping internal boundary layer at the Ocean front at this level, as observed on this day by Zhang et al. (2020, 2021), while the sinking would be due to its passage over the SBF gravity current head. For the next 6 h, it continued a slow movement northeastward to Flax Pond, producing its observed O_3 peak at 1200 m. The parcel that arrived at 1200 m at 0100 EST on 2 July was thus polluted as it slowly passed NYC from 1600 to 1900 EST on 1 July.

The concurrent 500 m parcel stayed close to its original height of 1000 m after leaving Pennsylvania (in an area west of NJ) at 0100 EST on 1 July. It then traveled southeastward for 12 h; by 1100 EST it had started a 4-h descent to 200 m over NJ. The descent probably started when it encountered the (overland) northwestern edge of the offshore surface H in Fig. 2c. At 1300 EST it made a sharp turn and flowed northeasterly, influenced by the northeastward flow from the northern edge of the H, eventually rising to 500 m at 1900 EST. For the next 12 h, it moved northeastward to Flax Pond, rapidly passing NYC 6-h after the 1200 m parcel. This rapid passage resulted in the relatively low O_3 at the 500 m level at Flax Pond. The 100 m air also originated in the same Pennsylvania area, but 400 m below that of the 500 m air. It likewise flowed southeastward for about 12 h, while slowly descending to 200 m. The latter part of the descent occurred as it encountered the offshore surface H in Fig. 2c, but more towards its northeastern edge. It thus executed a sharp 180° turn at 1300 EST away from the H and to the north. For the next 12 h, it moved northeastward to Flax Pond while maintaining its 100 m elevation. As it never passed NYC, its arrival at Flax Pond produced a near-surface O_3 minimum.

Back trajectories ending 12-h later at Flax Pond (Fig. 16b) show that the air producing its 1200 EST O_3 peak on 2 July at 1200 m (Fig. 15d) originated 24-h earlier from 12 km east of Flax Pond at a height of 200 m. It first flowed southward for 2-h at its original level, but rose quickly at about 1400 EST on 1 July to a height of 1250 m. Its upward motion was again due to that at the leading edge of the surface Ocean front. For the next 5-h, it moved seaward over the MBL in the upper-level SBF return flow. From 1900 to 0100 EST on July 2 it stagnated over the Ocean before reversing direction, and for the next 10-h moved northward to Flax Pond. It slowly descended to about 800 m throughout the 20-h period ending at 1100 EST, probably as the regional offshore H moved southward. It quickly rose to 1200 m during its last hour of travel due to the rapid upward motion at the SBF head, then located south of Flax Pond (Fig. 13). Its trajectory thus brought back to Flax Pond remnants of its near-surface high O_3 concentrations at the start of the trajectory 24-h before, and thus producing the observed peak at 1200 m on 2 July. The parcel only passed over land (i.e., LI) during the last hour of its

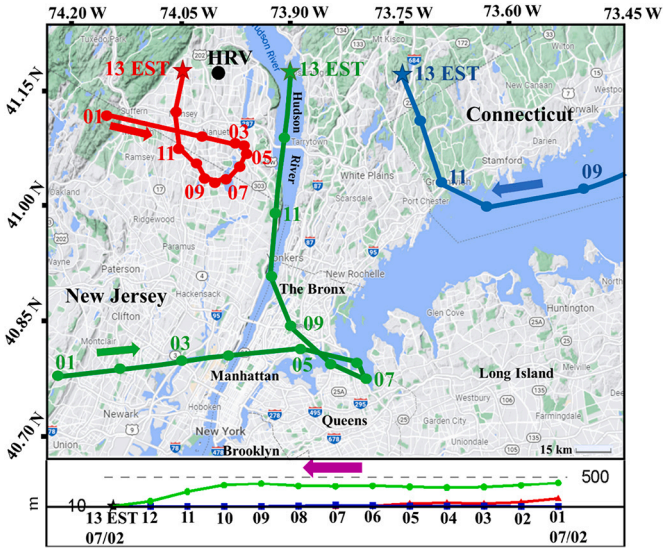

Fig. 17. As in Fig. 16, but ending over a Hudson River site (green) and at two nearby sites (red and blue) at 1300 EST on 2 July and at a receptor height of 10 m. (For interpretation of the references to colour in this figure legend, the reader is referred to the web version of this article.)

trajectory.

The 500 m parcel, however, originated at the surface over the Ocean at a point 130 km south of Flax Pond on 1 July at 1200 EST. It first flowed northeastward to Flax Pond for 13 h, still near the surface. During the next 10-h it, however, moved northwestward, reaching the southern LI shore at about 1000 EST. In its final hour, it continued northward over the Island but quickly ascended to 500 m as it was overtaken by the rapidly moving SBF. This low-level trajectory thus again recirculated high O_3 air back to Flax Pond, producing its observed 500 m peak, but again with an almost exclusively over water path. The 100 m parcel likewise originated over the Ocean area near the surface, but 30 km northeast of the 500 m parcel. It likewise flowed northeastward near-surface for about 13-h and then moved mainly westward (still near the surface) during most of its final 10-h. It rose to 100 m during its final hour, however, as it was broadsided by the northward moving SBF. This lowest trajectory thus also recirculated low O_3 air from the previous day back to Flax Pond.

A Hysplit 12-h back trajectory on 2 July that ended over the Hudson River (Fig. 17) at a location 10 km east of the HRV site shows that the air that associated with the 1300 EST surface O_3 peak at this nearby site (seen Fig. 11a) originated west of NYC at about 500 m. It first flowed eastward, passing the City at about 0700 EST at 400 m, when it reversed direction to move northwestward, thus again passing NYC. The reversal resulted as it encountered the complex flows at the narrow western edge of LI Sound. The air then moved northwestward for 3-h, crossing the River Valley at 1000 EST at much the same elevation. It then moved around the western edge of the NJ Palisades (shown in Fig. 1d), turning slightly eastward into the flow over the Valley after 1100 EST, consistent with the flow in Fig. 7c. Its descent to 10 m over the River had begun at 1000 EST and continued as it moved northward over the River, with its colder T-values and hence shallower PBL. Such channeling effects were also modeled in this Valley by Zhang et al. (1998).

The corresponding air arriving a location 5 km west of the HRV site originated at the NJ-NYS border at about 100 m. It first flowed southeastward for 3-h before making a 90° turn to the south and then moving northward for its final 4-h. It had moved to the surface during its first 2-h and remained at that level for the rest of the trajectory. The corresponding parcel arriving at a location 25 km east of the HRV site originated over the LIS at the surface and it remained at that level throughout its trajectory (the first 8-h of which are west of the figure domain). It flowed southwestward along the Connecticut coast for 10-h before making a sharp turn to the north as it encountered the Connecticut SB flow.

In summary, back trajectories ending at Flax Pond 12-h before the formation of its peak PBL O_3 showed that the air arriving there had slowly passed emission-rich NYC and thus brought early morning high pollution from the previous day. Similar trajectories ending 12-h later showed that the air in the upper-level O_3 peak had originated at the surface, just east of Flax Pond on the previous afternoon, and returned to the site with its 2 July SB flow. The 12-h back trajectories ending around the HRV site at 1300 EST on the episode day showed that the terrain channeling from the Hudson River Valley is narrow in extent, as sites 15 km on either site of the Valley did not show the transport from NYC seen as the HRV site.

4. Conclusion

The study analyzed meteorological and O_3 measurements collected in the NYC metropolitan area during a five-day period during the July 2018 LISTOS IOP field campaign. Data were obtained from an extensive surface network, as well as from PBL profiles at a coastal site on the north shore of LI. The period was characterized by a regional heat wave and an O_3 episode, both of which peaked on 2 July. The data were used to determine NYC impacts at the surface and within the PBL on regional temperature, wind, NO_2, and O_3 patterns, initially including multiple sea breeze fronts (SBFs) that ultimately combined into a single regional front.

Results showed that the synoptic forcing was dominated by an upper level, clear-sky high-pressure ridge centered northeast of NYC, far enough from the City that its subsidence inversion over NYC was weak and at a high elevation. Synoptic surface pressures on the episode day of 2 July showed an offshore high east of NYC, with low-speed onshore surface flows over the City that had changed from an along-shore direction on the previous day. Such conditions in urban coastal areas are conducive to the observed UHI, SBF, and regional photochemical O_3 conditions during the period. Regional surface temperatures showed that an NWS-defined heat wave began on 29 June and lasted for five days, until rain entered the area. The three-day EPA-O_3 episode peaked on 2 July, but it had started a day after the high temperatures began.

Early morning NYC NO_2 precursor emissions on 2 July produced localized maximum concentrations up to 60 ppb from 0400 to 0900 EST. The NYC UHI peaked at 8.3 °C at 0500 EST, but then weakened due to subsequent regional diurnal warming. The UHI produced a thermal low over the City that produced convergence at 0600 EST. The earliest NYC NO_2 emissions first drifted westward into NJ, while subsequent emissions became trapped in the UHI convergence for 3-h. Later emissions were pushed by a SBF into NJ and then transported northward around the Palisades hills into the Hudson River Valley. SBFs first came ashore at about 0700 EST, i.e., one from the Atlantic Ocean along the southern LI coast, with its middle section deformed to follow the northern edge of Jamaica Bay. The other two formed from flows from LI Sound: one a short-lived (2-h) weak front along northern LI coast and another on the southern Connecticut shore; 2-h later a fourth front formed on the NJ coast. The Ocean front moved inland fasted in the area northwest of the NY Bight, a westward extension of the Atlantic Ocean. Building-drag effects slowed and distorted the Ocean front over Manhattan for 2-h, but it finally passed the City at 1200 EST. All fronts had merged at 1400 EST and the combined front continued inland until 1800 EST when it reached the NJ hills and could not be found thereafter.

High O_3 surface concentrations first appeared at 0900 EST just west of NYC, co-located with the earlier NO_2 maximum. The subsequent rapid inland movement of the Ocean front beyond the NY Bight transported the peak further downwind into NJ during the next 2-h. As the Connecticut front continued northward, it coincided with the formation of a second (weaker) O_3 peak at HRV at 1100 EST, most likely due to photochemical processes in the northward-transported early morning precursor NO_2 emissions; a north-south ridge line connected the two peaks. Two weaker isolated peaks were also first seen at this time: one east of NYC over LI and another at a

NJ industrial area at the southwest domain edge. The two SBFs and O_3 ridge continued westward for the next 2-h, while values at HRV reached their highest level at any site, 145 ppb at 1300 EST, a value within the EPA's most extreme health impact concentrations. The two remaining fronts combined in central NJ by 1300 EST, while the mid-afternoon O_3 concentrations generally showed a normal diurnal decrease, except at the NJ industrial site, where they continued to increase for another 2-h. By 1600 EST the O_3 ridge had been replaced by a post-frontal "band" of high values at the edge of the network.

In summary, the study showed that its O_3 maxima were generally collocated with maximum temperature areas, and the high O_3 band was generally just behind the SBF. Early morning UHI-induced convergence into NYC, as well as later building-drag retardation of the SBF over the City, both slowed O_3 precursor transport from NYC. This delayed transport impacted the location, time evolution, and magnitude of the resulting downwind O_3 concentrations over NJ and at the newly identified Hudson River Valley peak. The study also showed that the western limit of NYC emissions and flow impacts extended to the NJ hills, at which point the O_3 and flow patterns probably blended into the regional episode and heat wave values.

Back trajectories ending at Flax Pond 12-h before the formation of its peak PBL O_3 value, showed that the air arriving at that site had slowly passed NYC. Similar trajectories ending 11-h later showed that the PBL peak originated at the surface at Flax Pond on the afternoon of 1 July. It had first flowed offshore/southward but rose quickly due to upward motion at an SBF gravity head. It continued seaward in the upper-level return flow above the gravity current, stagnating over the sea overnight, before reversing direction back to Flax Pond with the 2 July sea breeze. These trajectories thus show that the pollution in the observed PBL O_3 peak at Flax Pond on the episode day was in the air that passed NYC 36-h previously, arrived at Flax Pond before the start of the episode, and then recirculated in the sea breeze flow of that day. Additional back trajectories ending around the HRV O_3 site north of NYC at 1300 EST on 2 July showed channeling impact arising from the Hudson River Valley. The high episode peak O_3 air arriving at that site slowly passed twice over polluted NYC and then was transported around the Palisades hills west of the City northward towards the Hudson River, where it followed its narrow valley to the area of the O_3 peak.

The results of the current study are thus important as they answer the science questions posed above. The results have shown how the surface and PBL observations from the July 2018 LISTOS IOP can provide an improved understanding of how NYC impacts the movement of NO_2 precursor emissions, as it first traps them in an early morning UHI-induced convergence. They also have shown how these impacted transport patterns interact with the several SBFs that formed in the area along its complex coast to produce the several O_3 peaks at the surface and aloft. As the fronts moved inland, the regional heat wave was seen to exacerbate the surface O_3 peak that formed behind it, as well worsening as its health impacts.

As summer O_3 prediction is a significant challenge in and around large coastal cities, the current results should be useful in planning how to improve urban coastal environments and how to mitigate such environments in changing climates. Knowledge of the reduction of winds over cities and their retardation of SBFs, which both delay the inland cooling from such fronts, as well as impact their altered pollutant transport patterns, should significantly enhance urban planning processes in and around NYC, at other US urban areas, and for cities globally.

Future efforts should continue the analysis of the rich LISTOS observations. Numerical simulations of the event should involve the use of the urbanized WRF-Chem model, with a focus on NYC impacts on regional flow patterns and 3-D sea breeze frontal structures, as well as interactions with inert and photochemical pollutants. Such studies should also consider urban impacts on PBL convective processes along such SBFs (Pielke, 1974). Additional long-term climatological and short-term intensive field studies of NYC impacts on SBFs and O_3 are also needed, especially for fronts formed in otherwise calm circumstances and during opposing offshore flows. They should include surface sites in areas that require additional meteorological measurements. i.e., north of Jamaica Bay, as well as new NO_2 sites north of NYC and new O_3 sites both in the NJ hills and within the Hudson River Valley. Their PBL observations should include additional lidars, radars, ceilometers, flux towers, aircraft, and helicopter platforms.

Declaration of Competing Interest

The authors declare that they have no conflict of interest. The statements contained within the presentation are not the opinions of the funding agencies nor of the US government, but only reflect author opinions.

Acknowledgments

The authors would like to acknowledge the helpful technical comments of Jeff Freedman. The lead author was supported by the National Natural Science Foundation of China [grant number 41975004]; US National Science Foundation [grant number CBET-1832678]; and a China Scholarship Council grant. The work was also supported by NYSERDA [contract number 137482] and NES-CAUM [project number 2411], and by NOAA Educational Partnership Program/Minority-Serving Institutions [award number NA16SEC4810008] to the Center for Earth System Sciences and Remote Sensing Technologies (CESSRST) at CCNY. Contents are solely the responsibility of the author(s) and may not represent the official views of the sponsors. We acknowledge the free use of US EPA air quality and AQI data, the NOAA HYSPLIT model, NARR synoptic charts. and LISTOS ozonesonde data from the University at Albany, with support from the New York State (NYS) Energy and Development Authority Agreement [number 101132]. This work constitutes part of the Ph.D. dissertation of the lead author. The authors declare that they have no conflict of interest. The statements contained within the presentation are not the opinions of the funding agencies nor the US government but only reflect author opinions.

References

Automated Surface Observing System (ASOS) User's Guide, National Oceanic, and Atmospheric Administration, Department of Defense, Federal Aviation Administration, United States Navy, 1998. https://www.weather.gov/media/asos/aum-toc.pdf.

Bornstein, R.D., 1968. Observations of the urban heat island effect in New York City. J. Appl. Meteorol. 7, 575–582 doi: 10.1175/1520-0450(1968)007,0575: OOTUHI.2.0.CO;2.

Bornstein, R.D., 1987a. Urban barrier effects on mesoscale and synoptic systems. In: Paper presented at Third AMS Conference on Mesoscale Processes, Vancouver, British Columbia.

Bornstein, R.D., 1987b. Mean diurnal circulation and thermodynamic evolution of urban boundary layers. In: Modeling the Urban Boundary Layer, 53–93. Meteorological Society, Boston, MA, American.

Bornstein, R.D., Anderson, S.A., 1980. Sea breeze frontal slopes and vertical velocities over NYC. In: Paper Presented at 2nd AMS Conference on Coastal Meteor, Los Angeles, CA.

Bornstein, R.D., Johnson, D.S., 1977. Urban-rural wind velocity differences. Atmos. Environ. 11 (7), 597–604. https://doi.org/10.1016/0004-6981(77)90112-3.

Bornstein, R.D., Thompson, W.T., 1981. Effects of frictionally retarded sea breeze and synoptic frontal passages on sulfur dioxide concentrations in New York City. J. Appl. Meteorol. 20 (8), 843–858. https://doi.org/10.1175/1520-0450(1981)020<0843: EOFRSB>2.0.CO;2.

Bornstein, R.D., Imamura, R., González, J.E., Lebassi, B., 2012. Interactions of global-warming and urban heat islands in different climate-zones. National Security and human health implications of climate change. In: Fernando, H., Klaić, Z., McCulley, J. (Eds.), *NATO* Science for Peace and Security Series C: Environmental Security. Springer, Dordrecht, pp. 49–60. https://doi.org/10.1007/978-94-007-2430-3_5.

Boucouvala, D., Bornstein, R., 2003. Analysis of transport patterns during an SCOS97-NARSTO episode. Atmos. Environ. 37, 73–94. https://doi.org/10.1016/S1352-2310(03)00383-2.

Colle, B.A., Novak, D.R., 2010. The New York bight jet: climatology and dynamical evolution. Mon. Wea. Rev. 138 (6), 2385–2404. https://doi.org/10.1175/2009MWR3231.1.

Darby, L.S., McKeen, S.A., Senff, C.J., White, A.B., Banta, R.M., Post, M.J., Brewer, M.J., Marchbanks, R., Alvarez II, R.J., Peckham, S.E., et al., 2007. Ozone differences between near-coastal and offshore sites in New England: Role of meteorology. J. Geophys. Res.-Atmos. 112 (D16S91), 1–17. https://doi.org/10.1029/2007JD008446.

Ding, A., Wang, T., Zhao, M., Wang, T., Li, Z., 2004. Simulation of sea-land breezes and a discussion of their implications on the transport of air pollution during a multi-day ozone episode in the Pearl River Delta of China. Atmos. Environ. 38 (39), 6737–6750. https://doi.org/10.1016/j.atmosenv.2004.09.017.

Dou, J., Wang, Y., Bornstein, R., Miao, S., 2015. Observed spatial characteristics of Beijing urban climate impacts on summer thunderstorms. J. Appl. Meteorol. Climatol. 54, 94–105. https://doi.org/10.1175/JAMC-D-13-0355.1.

Dou, J., Bornstein, R., Miao, S., Sun, J., Zhao, Y., 2020. Observation and simulation of a bifurcating thunderstorm over Beijing. J. Appl. Meteorol. Climatol. 59 (12), 2129–2148. https://doi.org/10.1175/JAMC-D-20-0056.1.

Draxler, R.R., Hess, G.D., 1998. An overview of the HYSPLIT_4 modeling system for trajectories, dispersion, and deposition. Aust. Meteorol. Mag. 47 (4), 295–308.

Ferdiansyah, M.R., Inagaki, A., Kanda, M., 2020. Detection of sea-breeze inland penetration in the coastal-urban region using geostationary satellite images. Urban Clim. 31, 100586 https://doi.org/10.1016/j.uclim.2020.100586.

Frizzola, J.A., Fisher, E.L., 1963. A series of sea breeze observations in New York City Area. J. Appl. Meteorol. 2 (6), 722–739. https://doi.org/10.1175/1520-0450(1963)002<0722: ASOSBO>2.0.CO;2.

Gaffen, D., Bornstein, R.D., 1988. Case study of urban interactions with a synoptic scale cold front. Meteorog. Atmos. Phys. 38, 185–194. https://doi.org/10.1007/BF01054571.

Gaza, R.S., 1998. Mesoscale meteorology and high ozone in the Northeast United States. J. Appl. Meteorol. Climatol. 37 (9), 961–977 doi:10.1175/1520-0450(1998)037<0961: MMAHOI>2.0.CO;2.

Gedzelman, S.D., Austin, S., Cermak, R., Stefano, N., Partridge, S., Quesenberry, S., Robinson, D.A., 2003. Mesoscale aspects of the urban heat island around New York City. Theor. Appl. Climatol. 75, 29–42. https://doi.org/10.1007/s00704-002-0724-2.

Grimmond, C.B., 2007. Urbanization and global environmental change: local effects of urban warming. R. Geogr. Soc. 173, 83–88. https://doi.org/10.1111/j.1475-4959.2007.232_3.x.

Holton, J.R., 1992. An Introduction to Dynamic Meteorology. Academic, San Diego, CA, p. 511. Retrieved from. http://dca.ufcg.edu.br/DCA_download/An%20Introduction%20to%20Dynamic%20Meteorology.pdf.

Hsu, S.A., 1988. Coastal Meteorology. Academic Press, San Diego, CA, p. 260.

Hy-Eun, J., Soon-Hwan, L., Hwa-Woo, L., 2013. Characteristics of sea breeze front development with various synoptic conditions and its impact on lower troposphere ozone formation. Adv. Atmos. Sci. 30 (5), 1461–1478. https://doi.org/10.1007/s00376-013-2256-3.

Imamura, I.R., 1991. Observational Studies of Urban Heat Island Characteristics in Different Climate Zones, (Doctoral Dissertation). University of Tsukuba, Japan.

Lee, C., Martin, R.V., Donkelaar, A., Lee, H., Dickerson, R.R., Hains, J.C., et al., 2011. SO_2 emissions and lifetimes: estimates from inverse modeling using in situ and global, space-based (SCIAMACHI and OMI) observations. J. Geophys. Res.-Atmos. 116 (D6) doi:10.1029/2010JD014758Miller.

Lenschow, D.H., Pearson Jr., R., Stankov, B.B., 1981. Estimating the ozone budget in the boundary layer by use of aircraft measurements of ozone eddy flux and mean concentration. J. Geophys. Res. Oceans 86 (C8), 7291–7297. https://doi.org/10.1029/JC086iC08p07291.

Li, D., Bou-Zeid, E., 2013. Synergistic interactions between urban heat islands and heat waves: the impact in cities is larger than the sum of its parts. J. Appl. Meteorol. Climatol. 52 (9), 2051–2064. https://doi.org/10.1175/JAMC-D-13-02.1.

Loose, T., Bornstein, R.D., 1977. Observations of mesoscale effects on frontal movement through an urban area. Mon. Wea. Rev. 105 (5), 563–571. https://doi.org/10.1175/1520-0493(1977)105%3C0563:OOMEOF%3E2.0.CO;2.

Loughner, C.P., Allen, D.J., Pickering, K.E., Zhang, D.L., Shou, Y.X., Dickerson, R.R., 2011. Impact of fair-weather cumulus clouds and the Chesapeake Bay breeze on pollutant transport and transformation. Atmos. Environ. 45 (24), 4060–4072. https://doi.org/10.1016/j.atmosenv.2011.04.003.

Lyons, W.A., Sawdey, E.R., Schuh, J.A., Carby, R.H., Keen, C.S., 1981. An updated and expanded coastal fumigation model. In: Paper presented at 74th Meeting of the Air Pollution Control Association, Philadelphia, PA.

Melecio-Vázquez, D., Ramamurthy, P., Arend, M., González-Cruz, J.E., 2018. Thermal structure of a coastal-urban boundary layer. Bound.-Layer Meteorol. 169, 151–161. https://doi.org/10.1007/s10546-018-0361-7.

Mesinger, F., DiMego, G., Kalnay, E., Shafran, P.C., Ebisuzaki, W., Jović, D., et al., 2006. North American regional reanalysis. Bull. Amer. Meteorol. Soc. 87 (3), 343–360. https://doi.org/10.1175/BAMS-87-3-343.

National Weather Service, 2015. Natural Hazard Statistics. Accessed 20 November 2015. http://www.nws.noaa.gov/om/hazstats.shtmlP.

Novak, D.R., Colle, B.A., 2006. Observations of multiple sea breeze boundaries during an unseasonably warm day in metropolitan New York City. Bull. Amer. Meteorol. Soc. 87 (2), 169–174. https://doi.org/10.1175/BAMS-87-2-169.

Okabe, A., Boots, B., Sugihara, K., Chiu, S., 2000. Definitions and basic properties of Voronoi diagrams. In: Barnett, V., et al. (Eds.), Spatial Tessellations: Concepts and Applications of Voronoi Diagrams. John Wiley and sons, New York, NY, pp. 43–106.

Oke, T.R., Mills, G., Christen, A., Voogt, J.A., 2017. Urban Clim. Cambridge University Press, Cambridge, UK, p. 525.

Ongoma, V., Muthama, N.J., Gitau, W., 2013. Evaluation of urbanization influences on urban winds of Kenyan cities. Ethiop. J. Environ. Stud. Manag. 6 (3), 223–231. https://doi.org/10.4314/ejesm.v6i3.1.

Ortiz, L., González, J.E., Horton, R., Lin, W., Wu, W., Ramamurthy, P., Arend, M., Bornstein, R.D., 2019. High-resolution projections of extreme heat in New York City. Int. J. Climatol. 39 (12), 4721–4735. https://doi.org/10.1002/joc.6102.

Pielke, R.A., 1974. A three-dimensional numerical model of the sea breezes over South Florida. Mon. Wea. Rev. 102 (2), 115–139. https://doi.org/10.1175/1520-0493(1974)102<0115: ATDNMO>2.0.CO;2.

Pullen, J., Holt, T., Blumberg, A.F., Bornstein, R.D., 2007. Atmospheric response to local upwelling in the vicinity of New York-New Jersey Harbor. J. Appl. Meteorol. Climatol. 46 (7), 1031–1052. https://doi.org/10.1175/JAM2511.1.

Rao, P., Fuelberg, H.E., 2000. An investigation of convection behind the Cape Canaveral Sea-breeze front. Mon. Wea. Rev. 128 (10), 3437–3458. https://doi.org/10.1175/1520-0493(2000)128<3437: AIOCBT>2.0.CO;2.

Ritchie, H., Roser, M., 2018. Plastic Pollution. Our World in Data. https://www.researchgate.net/deref/https%3A%2F%2Fourworldindata.org%2Fplastic-pollution.

Seaman, N.L., Michelson, S.A., 2000. Mesoscale meteorological structure of a high-ozone episode during the 1995 NARSTO-Northeast study. J. Appl. Meteorol. 39 (3), 383–398. https://doi.org/10.1175/1520-0450(2000)039<0384: MMSOAH>2.0.CO;2.

Sibson, R., 1981. A brief description of natural neighbor interpolation. In: Barnett, V. (Ed.), Interpreting Multivariate Data. John Wiley and Sons, New York, NY, pp. 21–36.

Simpson, J.E., 1994. Sea Breeze and Local Wind. Cambridge University Press, NY, p. 28.

Simpson, J.E., 1997. Gravity Currents in the Environment and the Laboratory. Cambridge University Press, NY, p. 244.

Simpson, J.E., Mansfield, D.A., Milford, J.R., 1977. Inland penetration of sea-breeze fronts. Quart. J. Roy. Meteorol. Soc. 103 (435), 47–76. https://doi.org/10.1002/qj.49710343504.

Stewart, I.D., Oke, T.R., 2012. Local climate zones for urban temperature studies. Bull. Amer. Meteorol. Soc. 93 (12), 1879–1900. https://doi.org/10.1175/BAMS-D-11-00019.1.

Tan, J., Zheng, Y.F., Tang, X., Guo, G.Y., Li, L.P., Song, G.X., Zhen, X., Yuan, D., Kalkstein, A.J., Li, F., 2010. The urban heat island and its impact on heat waves and human health in Shanghai. Int. J. Biometeorol. 53, 75–84. https://doi.org/10.1007/s00484-009-0256-x.

Technique Specification Package 88-21-R2 for AWIPS-90 RFP Appendix G Requirements Numbers: Quality Control Incoming Data, 1994. AWIPS Document Number TSP-032-1992R2, NOAA, National Weather Service, Office of Systems Development. https://madis.ncep.noaa.gov/madis_raob_qc_notes.shtml.

Tijm, A.B.C., van Delden, A.J., 1999. The role of sound waves in sea-breeze circulation. Quart. J. Roy. Meteorol. Soc. 125, 1997–2018. https://doi.org/10.1002/qj.49712555805.

United Nations, Department of Economic and Social Affairs, Population Division, 2018. World Urbanization Prospects: The 2018 Revision (ST/ESA/SER.A/420). United Nations, New York, NY. Retrieved from: http://www.un.org/.

U.S. Geological Survey. Global Multi-resolution Terrain Elevation dataset at Earth Resources Observation and Science (EROS) Center. https://www.usgs.gov/centers/eros/science.

Van Rossum, G., Drake, F.L., 2009. Python 3 Reference Manual. CreateSpace, Scotts Valley, CA.

Wentworth, G.R., Murphy, J.G., Sills, D.M., 2015. Impact of lake breezes on ozone and nitrogen oxides in the Greater Toronto area. Atmos. Environ. 109, 52–60. https://doi.org/10.1016/j.atmosenv.2015.03.002.

Yamamoto, Y., Ishikawa, H., 2020. Influence of urban spatial configuration and sea breeze on land surface temperature on summer clear-sky days. Urban Clim. 31, 100578 https://doi.org/10.1016/j.uclim.2019.100578.

Zhang, J., Rao, S.T., Daggupaty, S.M., 1998. Meteorological processes and ozone exceedances in the Northeastern United States during the 12-16 July 1995 episode. J. Appl. Meteorol. 37 (8), 776–789 doi:10.1175/1520-0450(1998)037<0776: MPAOEI>2.0.CO;2.

Zhang, J., Ninneman, M., Joseph, E., Schwab, M.J., Shrestha, B., Schwab, J.J., 2020. Mobile laboratory measurements of high surface ozone levels and spatial heterogeneity during LISTOS 2018: evidence for sea breeze influence. J. Geophys. Res.-Atmos. 125 (11), 1–19. https://doi.org/10.1029/2019JD031961.

Zhang, J., Mak, J., Wei, Z., Cao, C., Ninneman, M., Marto, J., Schwab, J., 2021. Long Island enhanced aerosol event during 2018 LISTOS: association with heatwave and marine influences. Environ. Pollut. 270, 116299. https://doi.org/10.1016/j.envpol.2020.116299.

Zhong, S.Y., Takle, E.S., 1992. An observational study of sea- and land- breeze circulation in an area of complex coastal heating. J. Appl. Meteorol. Climatol. 31 (12), 1426–1438. https://doi.org/10.1175/1520-0450(1992)031<1426: AOSOSA>2.0.CO;2.